Cláudia Sofia Rodrigues Ferreira

Bachelor in Micro and Nanotechnologies Engineering

Development of PNA-DNA Field-Effect Transistor-based biosensors

Dissertation submitted in partial fulfilment of the requirements for the degree of
Master of Science in
Micro and Nanotechnologies Engineering

Adviser: Dr. Pedro Estrela, Senior Lecturer, University of Bath

Co-adviser: Dr. Elvira Fortunato, Full Professor, Faculty of Science and Technology, NOVA University of Lisbon

FACULDADE DE
CIÊNCIAS E TECNOLOGIA
UNIVERSIDADE NOVA DE LISBOA

September, 2017

"Happiness can be found, even in the darkest of times, if only one remembers to turn on the light." –The Prisoner of Azkaban

Acknowledgments

I would firstly like to thank my supervisor Dr. Pedro Estrela, for allowing me to be a part of his research group in the University of Bath and for the invaluable guidance and support over these months. I would also like to thank my co-supervisor Dr. Elvira Fortunato for her knowledge and help over the years as well as the help in finding this opportunity. To the biosensors group in the University of Bath, I would like to thank for the open arm welcome I received as well as for all of the help in the lab and support. Special thanks to Şerife Üstüner for teaching me everything I needed to know to work on my own as well as for the patience and moral support when all seemed to be failing. To Dr. Pawan Jolly for using his time helping in my measurements, for the nice chats and lovely meals. To Jahnavi Jha for the help in the fabrication of electrodes and the motivational talks. To Erasmus plus for supporting me financially. Ao Prof. Dr. Rodrigo Martins e à Prof. Dra. Elvira Fortunato pela criação e promoção do curso de Engenharia Micro e Nanotecnologias.

Gostaria desde já agradecer a todas as pessoas que fizeram parte, direta ou indiretamente, do meu percurso neste curso, quer eu as refira aqui ou não, nada disto seria possível sem o vosso apoio incondicional.

Aos meus amigos da residência, obrigada pelos momentos de descontração na cozinha e sala de estudo, pelas pré-festas, pela companhia quando tinha de fazer diretas, pelas idas a Lisboa e ao fórum, agradeço por todo o apoio, ajuda e risadas ao longos destes anos. Um especial agradecimento ao (José) Miguel e Sabrina por todas as noites de fritanço, por todas as conversas e loucuras e por saber que tinha sempre um ombro amigo disponível.

À Joana, por sempre me apoiar e aturar mesmo quando estava exausta e continuar do meu lado mesmo quando não vinha a casa durante meses, pelas idas a Lisboa, pelos pequenos-almoços na Panitejo, pelas longas conversas sobre vida e tretas que mais ninguém percebe, pelas idas ao cinema, por finalmente ir ao UK só para me ver, amizades assim não se encontram todos os dias e espero que continuemos assim por muitos anos. A todos os meus amigos pela paciência e apoio demonstrados ao longo deste período da minha vida.

Por último e de todo o mais importante, gostaria de agradecer á minha família por todo o apoio e encorajamento, especialmente ao meu pai e avó. Ao meu pai, pela incrível dedicação, amor, carinho e paciência para me aturar (mesmo quando não paro quieta e calada), pelas doses de motivação diária em todos os aspetos da minha vida, pelas conversas perlongadas ao telefone ou ao Skype, por me ensinar que nada na vida se obtém sem esforço e muito trabalho. Basicamente, obrigada por seres o melhor pai de sempre e por teres estado sempre ao meu lado ao longo da minha vida. À minha avó, por sempre ter tratado de mim não apenas como uma neta, mas como uma filha, especialmente, mas não apenas quando o meu pai não podia estar presente, pelo amor, preocupação, carinho e uma dose ainda maior de paciência, pelas tabuadas e por sempre teres feito a comida que mais gosto.

Abstract

The high demand for devices with higher sensitivity as well cost-efficiency has put tremendous pressure on the biosensors field. The numerous advantages of Field effect transistors (FETs) such as small size, fast response, label free response, and possibility of on-chip integration of biosensor arrays with a future prospect of low-cost mass production, make their development highly desirable. An electrochemical deoxyribonucleic acid (DNA) biosensor using a synthesized ferrocene-based DNA intercalator as a redox marker was investigated. A peptide nucleic acid (PNA) was employed as a capture probe and co-immobilized on electrodes with 6-mecarpto-hexanol (MCH) to control the surface density of the probe, and hybridized with complementary DNA. After hybridization, a ferrocene-based intercalator was introduced to bind with the PNA-DNA duplex and change the surface potential. Biologically sensitive field-effect transistor (BioFET) was used to monitor the DNA recognition. As confirmation, electrochemical impedance spectroscopy (EIS) was also used to characterize the different modification steps. Differential pulse voltammetry (DPV) was employed to evaluate the electrochemical signal of the intercalator, related to its interaction with the PNA-DNA duplex. An optimization of the PNA probe surface density was also tried, with the density being controlled by the MCH ratio in solution. Hybridization of PNA-DNA with a PNA/MCH ratio of 1:29 was obtained in BioFET and EIS, the employed intercalator showed to have poor stability, both in application in BioFET as in DPV. Different ratios were tried and the use of different electrodes was also exploit.

Keywords: field-effect-based sensors; peptide nucleic acid; ferrocene-based intercalator.

Resumo

A elevada procura por dispositivos com maior sensibilidade, bem como eficiência de custos, co-locou uma tremenda pressão sobre o campo dos biossensores. As inúmeras vantagens dos transístores de efeito de campo (FETs), tais como o tamanho reduzido, a resposta rápida, a resposta livre de rótulos e a possibilidade de integração de matrizes de biossensor no chip com uma perspetiva futura de produção em massa de baixo custo, tornam o seu desenvolvimento altamente desejável. Um biossensor de ácido desoxirribonucleico (ADN) eletroquímico utilizando um intercalador de ADN sintetizado baseado em ferrocene, como marcador redox, foi investigado. Ácido peptídonucleico (APN) foi utilizado como sonda de captura e co-imobilizado em elétrodos com 6-mecarpto-hexanol (MCH) de forma a controlar a densidade superficial da sonda e hibridizado com ADN complementar. Após hibridação, um interca-lador à base de ferrocene foi introduzido para se ligar ao duplex APN-ADN e alterar o potencial super-ficial. O transístor de efeito de campo biologicamente sensível (BioFET) foi utilizado para monitorizar o reconhecimento do ADN. Como confirmação, espectroscopia eletroquímica de impedância (EEI) tam-bém foi utilizada para caracterizar as diferentes etapas de modificação. Voltametria de pulso diferencial (VPD) foi usada de forma a avaliar o sinal eletroquímico do intercalador, relacionado com a interação com o duplex APN-ADN. Uma otimização da densidade da superfície da sonda APN também foi ten-tada, sendo a densidade controlada pela relação com o MCH em solução. A hibridação de APN-ADN com uma relação APN / MCH de 1:29 foi obtida em BioFET e EEI e o intercalador utilizado mostrou ter baixa estabilidade, tanto na aplicação em BioFET como em VPD. Diferentes índices foram testados e o uso de diferentes elétrodos também foi explorado.

Contents

List of Figures

List of Tables

Abbreviations

a.c.	Alternating current
BioFET	Biologically-sensitive Field Effect Transistors
CPE	Constant Phase Element
d.c.	Direct current
DMSO	Dimethyl Sulfoxide
DNA	Deoxyribonucleic Acid
DPV	Differential Pulse Voltammetry
EIS	Eletrochemical Impendance Spectroscopy
FET	Field effect transistor
ISFET	Ion Sensitive Field Effect Transistor
MCH	6-mercapto 1-hexanol
PB	Phosphate Buffer
PNA	Peptide Nucleic Acids
SAM	Self Assembled Monolayer
ss-DNA	Single Stranded Deoxyribonucleic Acid

Symbols

A	Ampere
CPE	Constant Phase Element
h	Hour
Hz	Hertz
M	Molar
min	Minute
ω	Angular frequency
Pt	Platinum
Rct	Charge transfer resistance
Rs	Solution Resistance
t	Time
V	Volts
V_{DS}	Voltage between Source and Drain
V_{GS}	Voltage between Source and Gate
Vth	Threshold Voltage
W	Warburg element
Z	Impedance
Δ	Variation
ϕ	Electrostatic potential
χ_{int}	Interface Surface Dipole
ψ_{dl}	Electrochemical double-layer potential

Motivation and Objectives

Over the years, biosensors have become a major topic of scientific interest wide ever-growing potential applications. This growth as given rise to a vast multidisciplinary area of research that combines biology, analytical chemistry, physics and bio-electronics. Nowadays, biosensors have a wide range of areas of application, such as environmental monitoring, food control, security, forensic science and other areas. However, special reference as to be given to medical related applications, such as biomedical diagnosis, point-of-care monitoring of treatment and disease progression and drug discovery. In recent years, many new ways of detection, quantification and monitoring of different biological and chemical compounds have been studied and, in medical related applications, nucleic acids biosensors are becoming invaluable tools for detecting target genes responsible for diseases, or pollution, in various fields. Therefore, improvement of the detection of deoxyribonucleic acid (DNA) hybridisation is of significant scientific and technological importance, as well as the improvement of the sensitive layer and mechanisms of transduction for detection of bimolecular recognition.

The main goal of this thesis was to develop a biologically sensitive field effect transistor (BioFET) biosensor with an extended gold working electrode which would be functionalized with a peptide nucleic acid (PNA), employed as a probe and co-immobilized with 6-mecarpto-hexanol (MCH) to control the surface density of the probe. Following immobilization, incubation with the complementary DNA to allow hybridization was done and the addition of a ferrocene-based intercalator introduced to bind with the hybridized duplex and change the surface potential. Electrochemical impedance spectroscopy and DPV were used as confirmation steps for the PNA-DNA hybridization and investigation of the binding of the intercalator, respectively.

In the second part of this thesis, the goal was to perform the optimization of the PNA/MCH ratio to obtain the highest formation of PNA-DNA possible and, thus, highest change in potential. Additionally, the in-house fabrication and study of evaporated gold electrodes was also done as opposed to industrial bought electrodes.

1   Introduction

1.1   Biosensors: History, definition and basic components

The biosensor field has grown enormously ever since the first report of the biosensor concept by Leland C. Clark Jr., in 1962, with the development of the first glucose sensor and the enhancement of electrochemical sensors with enzyme-based transducers (Clark and Lyons, 1962). They have become a more attractive tool due to their ability to carry out rapid, direct, accurate analysis in point of care or on-site, low cost, fast response and ease of miniaturization (Bala and Gorski, 2016). This leads to the development of various applications of this type of devices, among them are biomedical, industrial, food and beverage, agricultural, environmental, forensic, security and defence, and toxicity monitoring.

A biosensor can be defined as a compact analytical device, which converts chemical information, from the concentration to total composition analysis, of a target substance of interest that needs detection, the analyte, into proportional electrical signals (Thévenot *et al.*, 2001). They usually are composed of two basic components connected in series: a bioreceptor and a physicochemical transducer. The bioreceptor, also designated a recognition element/system, is a molecule that interacts with the target analyte, selectively recognising and binding to it, which produces a physico-chemical change. The main purpose of the bioreceptor is to provide specificity and selectivity to minimize interferences from other sample components, thus the choice of the biological element in the recognition system is of utmost importance (Schöning and Poghossian, 2002). The nature of the target analyte must be taken into consideration, as well as its concentration in the sample, the presence or absence of interfering substances, and whether the measurement is discrete, real-time or continuous (Lowe, 2008). In general, the selection of the recognition element should be made according to the analytical method under development and intended application. Examples of recognition elements include enzymes, nucleic acids ((DNA, RNA, PNA, etc.), whole cells, synthetic receptors or binding proteins, such as antibodies, which are immobilized onto the surface of the transducer. The surface where the recognition element is immobilized is also a sensitive parameter. Depending on the measuring mode in use, a wide range of different materials can be chosen as surface. Among them are gold, silver, diamond, graphene and carbon nanotubes.

The transducer or detector is the element that detects and converts bio-recognition event, caused by the interaction between the bioreceptor and the analyte, into a measurable signal. This conversion process is known as signalisation. Either optical or electrical signals are the most commonly produced and are usually proportional to the amount of analyte–bioreceptor interactions (Bhalla *et al.*, 2016).

A biosensor can also have a signal processor which collects, amplifies, and displays the signal produced by the transducer (Ronkainen, Halsallb and Heinemanb, 2010).

The performance of a biosensor is usually evaluated based on its sensitivity, limit of detection (LOD), linear and dynamic ranges, selectivity and stability during operation and overtime. The response should be accurate, precise, reproducible and linear over the concentration range of interest, without dilution or concentration (Grieshaber *et al.*, 2008).

1.2   Classification

Biosensors can be distinguished either by their type of biorecognition system, their transducer mechanism or a combination of these two.

1.2.1   Biorecognition system

Biosensors can be divided into two main categories based on the nature of the biorecognition process: biocatalytic and affinity biosensors. Biocatalytic sensors are based on a reaction catalysed by macromolecules, which incorporates biological elements such as enzymes, whole cells (micro-organisms, such as bacteria or fungi) or tissue that recognize the target analyte and produce electroactive species or some other detectable outcome (Thévenot *et al.*, 2001). Affinity sensors are based on specific chemical binding. They use the selective and strong binding of macromolecules or organized molecular assemblies that have either been isolated from their original biological environment or engineered such as antibodies, membrane receptors, or oligonucleotides, with a target analyte to produce a measurable electrical signal (Ronkainen, Halsallb and Heinemanb, 2010).

1.2.1.1   Nucleic Acids Based Biosensors

The use of nucleic acids recognition layers in biosensor design is gaining increasing attention, mainly due to their wide field of possible uses and are now recognized as invaluable tools for detecting target genes responsible for diseases, or pollution, in various fields (DeRisi, Iyer and Brown, 1997; Yang *et al.*, 2015). A nucleic acid sensor is typically based on the binding ability of an immobilized nucleic acid layer (the probe) with a complementary DNA sequence (the target). Exposure of the sensor to a sample containing the target results in the formation of the hybrid on the surface. Electrochemical, optical or frequency monitoring of this duplex formation can thus result in a useful analytical signal (Joseph Wang, 1998). Several types of nucleic acids have been used as probe, which are grafted to the substrate surface via physical or electrochemical adsorption, self-assembly immobilization, biotin-avidin interactions, entrapment methods or covalent attachment (Gaiji *et al.*, 2017). These probes include single-stranded DNA (deoxyribonucleic acid) (Gao *et al.*, 2011), locked nucleic acid (LNA) (Wang *et al.*, 2011) and peptide nucleic acid (PNA) (Keighley *et al.*, 2008), to which a further in-deep look will follow.

1.2.1.1.1   Peptide nucleic acid

Peptide nucleic acid (PNA) was first described by Nielsen et al. in 1991(Nielsen *et al.*, 1991). PNA is a DNA analogue, in which the entire negatively-charged sugar-phosphate backbone of DNA has been replaced by an uncharged backbone consisting of repeated N-(2-aminoethyl) glycine units. The four natural nucleobases (adenine, cytosine, guanine, and thymine) come off the backbone at equal spacing to the DNA bases. A methyl carbonyl linker connects natural as well as unusual (in some cases) bases to the central amine of the backbone (Hyrup and Nielsen, 1996). Despite all these variations from natural nucleic acids, PNA still binds to its complementary oligonucleotides sequence (Ray and Nordén, 2000). PNA exhibits superior structural properties and hybridization with higher affinity and specificity making it superior to natural nucleic acids for use as a probe in sequence-specific hybridization, which open up many important biological and diagnostic applications not achievable otherwise. It has been shown that the PNA binding to complementary oligonucleotides obeys the Watson-Crick base-pairing

rules with the PNA and DNA strands joined via hydrogen bonds (Figure 1.1 - **Schematic chemical model of PNA (red) hybridized with DNA (blue) in antiparallel orientation with the hydrogen bonding between**
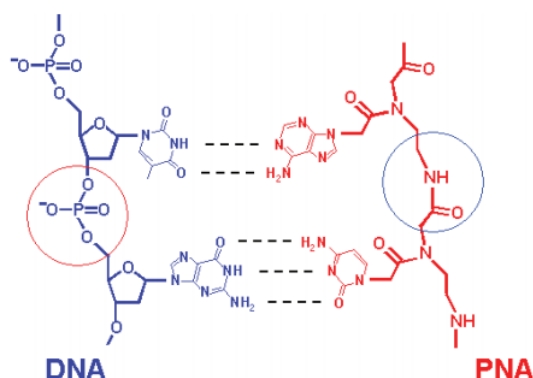
Figure 1.1 - Schematic chemical model of PNA (red) hybridized with DNA (blue) in antiparallel orientation with the hydrogen bonding between complementary nucleobases depicted by dotted lines. Adapted from (Mateo-Mart and Pradier, 2010).

complementary nucleobases depicted by dotted lines. Adapted from (Mateo-Mart and Pradier, 2010).) (Egholm *et al.*, 1993).

PNA has outstanding chemical and thermal stability, are non-ionic, achiral molecules, which thereby avoids problems of enantiomeric purity, and insensitive to enzymatic biodegradation by nucleases or peptidases, hence offering high biological stability (Demidov *et al.*, 1994). Additionally, thiol-modified PNA is able to form a self-assembled monolayer on the gold surface (Bala and Gorski, 2016). Due to the neutral backbone, there is a lack of electrostatic repulsion between the PNA and DNA strands, comparing to that existing between two negatively charged DNA oligomers, and hence a higher thermal stability of PNA/DNA duplexes. Also due to the neutral backbone, the thermal stability of the resulting PNA/DNA duplex is independent of the ionic strength of the solution in which hybridisation is performed (J Wang, 1998).

1.2.2 Transducer

Transduction can be accomplished via a great variety of methods. Optical biosensors are an example, in which the transduction process induces a change in the phase, amplitude, polarization, or frequency of the input light in response to the physical or chemical change produced by the biorecognition process (Vo-Dinh and Cullum, 2008). Another example of biosensors that can be classified by its mechanism of transduction are the electrochemical biosensors which are the focus of this work and will be addressed in-depth in the following section.

1.3 Electrochemical Biosensors

The electrochemical biosensors principal is that the electron flow between an electroactive species and an electrode surface, produced by a chemical reaction, and causes some change in the electrical properties of the solution. This change can be sensed and used both for qualitative and quantitative analysis (Mohanty and Koucianos, 2006). Some of the key advantages of electrochemical detection as transducer relies on the low cost, ease of use, portability, simplicity of construction, fast performance, excellent detection limits and possibility of miniaturization (Bala and Gorski, 2016).

This kind of biosensors usually requires a reference electrode, a counter or auxiliary electrode and a working electrode. The reference electrode is used to maintain a known and stable potential so in order to do so it must be kept at a distance from the reaction site. The working electrode serves as the

transduction element in the biochemical reaction. The counter electrode establishes a connection to the electrolytic solution so that a current can be applied to the working electrode. These electrodes should be both conductive and chemically stable. Therefore, platinum, gold, carbon and silicon compounds are commonly used, depending on the analyte (Grieshaber *et al.*, 2008).

Electrochemical sensors can be classified taking into account the electrochemical detection techniques used, in other words, considering the characteristics of the signal obtained by the transducer. If the reaction generates a measurable current due to the reduction or oxidation of electroactive species then the technique is amperometric, if it alters the conductive properties of the medium between the electrodes then the technique is conductometric, if it generates a measurable potential or charge accumulation it is a potenciometric technique. Another detection technique is impedimetric, which measures impedance (both resistance and reactance) and field-effect which uses transistor technology to measure current as a result of a potentiometric effect at a gate electrode (Grieshaber *et al.*, 2008). A more detailed description of the last detection technique will be given in the following sections.

1.3.1 Impedimetric sensors

Electrochemical Impedance Spectroscopy (EIS), ever since it was first described by Lorenz and Schulze in 1975 (Lorenz and Schulze, 1975), has become the most common technique used to monitor both resistance and reactance in impedimetric biosensors (Ronkainen, Halsallb and Heinemanb, 2010).

It measures the resistive or capacitive properties of materials after perturbation of the system by a small amplitude varying sinusoidal potential (Ronkainen, Halsallb and Heinemanb, 2010). The perturbation generates a current which is measured. By varying the frequency of the applied potential over a wide range of frequencies, the complex impedance of the system, which is the sum of the real and imaginary impedance components, can be calculated as a function of the frequency (Grieshaber *et al.*, 2008). In simplistic terms the real part is often linked to resistive processes and the imaginary part to capacitive processes. Therefore, the impedance Z is the quotient of the voltage – time function U(t) and the resulting current – time function I(t), as shown in Equation 1.

$$Z(t) = \frac{U(t)}{I(t)} = \frac{U_0 \sin(\omega t)}{I_0 \sin(\omega t + \phi)} = \frac{1}{Y}; \ \omega = 2\pi f \tag{1}$$

Where U_0 and I_0 are the maximum voltage and current signals, f is the frequency, t the time, φ the phase shift between the voltage–time and current–time functions, and Y is the complex conductance or admittance. The impedance is a complex value, since the current can differ not only in terms of the amplitude but it can also show a phase shift compared to the voltage – time function. Thus, the value can be described either by the modulus and the phase shift or by the real part and the imaginary part of the impedance (Lisdat and Schäfer, 2008). It allows to obtain detailed information about the physico-chemical changes that take place when an analyte binds to a bioreceptor immobilised on an electrode. Information such as charge transfer processes from the solution to the electrode surface, conductivity films, diffusion transport of species to and from the bulk solution and double layer capacitance formation and modification (Hammond *et al.*, 2016).

1.3.2 Biologically Sensitive Field Effect Transistor

Biologically Sensitive Field Effect Transistor (BioFET) is a field-effect transistor in which the gate is functionalized with different biological recognition elements. Initially these devices were classified as potentiometric sensors, since the detection mechanism is based on a potential or charge variation at the transducer when placed in contact with an electrolyte, these were separated into a new class of

6

electrochemical biosensors (Thévenot *et al.*, 2001). BioFETs can be simply constructed from an Ion-Sensitive Field Effect Transistor (ISFET) by modifying the gate or coupling it with different biological recognition elements. The choice of this bio-recognition elements, which are chemically or electrostatically bound to the transducer surface, is critical to the biosensor performance and should provide specific interaction with target molecules, minimize non-specific binding and, in some cases, facilitate a charge transfer (Pachauri and Ingebrandt, 2016). Field Effect Transistor (FET) is a type of transistor which consists of three terminals (electrodes): the source, the gate, and the drain. The device consists of a channel through which electrons or holes flow from the source to the drain by application of an electric field in the gate, which controls the conductivity (Hosseini, Tavallaei and Hosseini, 2015). In an n-channel FETs the carriers are electrons while in a p-channel FETs the carriers are holes. By varying the voltage applied to the gate, relatively to the source and drain electrode, which generates the electric field, control of the current between the source and drain conductivity is achieved (Pachauri and Ingebrandt, 2016).

In the case of a n-type transistor, the turn-on state is achieved when the electron-current (I_D) enters the drain and exits the source. When the potential applied across the gate and the source (V_{GS}) is larger than the threshold voltage (Vth) of the device (V_{GS}>Vth), a conducting channel is formed between the source and the drain. The Vth is the minimum voltage that is needed between the gate and source to create the channel. Additionally, if a voltage is applied between the drain and source (V_{DS}>0) a current (I_D) begins to flow through the channel. The presence of a sufficient positive or negative potential at the gate would either attract or repel charge carriers in the conduction channel. This would either fill or empty the depletion region of charge carriers and thus form or deform the effective electrical dimensions of the conducting channel. So, by changing V_{GS} the conductivity of the channel is modulated and thereby I_D is altered. In linear mode, when V_{DS}< V_{GS}, a FET operates much like a variable resistor to switch between conductive and non-conductive states. However, in saturation mode, a FET operates as a constant-current source and is often used as a voltage amplifier. In this mode the level of constant current is determined by the V_{GS} (Grieshaber *et al.*, 2008).

Some of the basic mechanisms of potential generation for BioFETs include catalytic reaction product (e.g., between an enzyme and its substrate), surface polarisation effects or change of dipole moments (e.g. DNA hybridisation) and potential changes that are coming from living biological systems as a result of more sophisticated (bio-)chemical processes (e.g., action potential of nerve cells) (Estrela, 2015)

BioFETs can be classified according to the biorecognition element that is used for detection. They can be divided in: enzyme-modified FET (EnFET); immunologically modified FET (ImmunoFET); DNA-modified FET (DNA-FET); cell-based FET (or cell-potential FET (CPFET)); and 'beetle/chip' FET (Schöning and Poghossian, 2006).

1.3.3   Intercalators

Various strategies have been suggested for the development of electrochemical sensors. In electrochemical nucleic acids based sensors, label-free methods, which are directly based on the electroactivity inherent to some nucleotides, and indirect label-methods (Wang and Kawde, 2001), which involve the use of electroactive markers and labels such as enzymes, nanoparticles and redox indicators and intercalators. The most widely employed are electroactive indicators containing organometallic or organic moieties, which connect directly and selectively to the nucleic acid sequences by electrostatic interactions, groove binding or intercalating interaction (Gaiji *et al.*, 2017). Intercalator can be define as

an organic small sized DNA binding molecule which present a characteristic structure with a planar polycyclic ring (Gaiji *et al.*, 2017). This allows them to fit between adjacent base pairs of the double helix structure without destroying hydrogen bonds. Therefore, such intercalators should be able to discriminate between double- and single-stranded DNA (Takenaka *et al.*, 2000).

2 Materials and Methods

2.1 BioFET measurements

Two different gold electrodes were used. Thin-film double metal-based electrodes, purchased from Micrux Technologies (Oviedo, Spain), and evaporated gold electrodes prepared in-house on glass slides.

2.1.1 Setup

To carry out the Bio-FET measurements, an extended-gate FET sensor was fabricated. To do so, the gold electrodes, fixed in a flow cell, were connected via a metal wire to the gate of an n-type MOSFET structure, which transduces the binding events on the electrode into electrical signals. In the case of the evaporated electrodes, an external reference electrode was used to apply the gate voltage. The FET readings were taken using an Agilent B1500A HR CMU Semiconductor Device Analyser. The threshold voltage of the transistor was 0.82 V. The length by width of the transistor was 10×2 µm. To operate the transistor for measurements, a V_{DS} of 50 mV was applied and V_{GS} was swept from 0 to 3 V.

Further detail on the setup and electrodes used can be found in Appendice A.

2.1.2 Fabrication and Hybridization of PNA-based Biosensor

The electrodes were sequentially cleaned by sonication in acetone, 2-Propanol and ultra-pure water for 3 min. Finally, thoroughly rinsed with ultra-pure water to remove any remaining particle residues and dried in a nitrogen stream. Evaporated electrodes were firstly subjected to UV-light for 10 min. Thereafter, the cleaned electrodes surfaces were exposed to different ratios of thiolated PNA to MCH immobilization solution. The short-chain thiol spacer, MCH, is commonly adopted to suppressed non-specific adsorption and to assure a "stand up" position of the PNA sequence, convenient for hybridization (Paleček and Bartošík, 2012). The immobilization solution was prepared using a protocol adapted from (Jolly *et al.*, 2015). The thiol terminated PNA sequence HS-$(CH_2)_6$-AEEA-TTT TTT TTA ATA CTA ACA CTG C (Cambridge Research Biochemical, UK) samples were prepared in a solution containing DMSO (Sigma Aldrich, UK) and ultra-pure water [20% and 80% (v/v)]. AEEA (2-aminoethoxy-2-ethoxy acetic acid is the short linker molecule used to join PNA strands. Concentrated solution of MCH was prepared in pure ethanol and further diluted to the desired concentrations in the DMSO-water mixture. Before immobilization, the PNA-MCH mixture was heated to 50 °C for 10 min, so that the PNA would be better dissolved in the solution and as described in the literature (Jolly *et al.*, 2015). The electrodes were then left overnight in a humidity chamber at 4 °C for preparation of the compact SAM layer. After immobilization, electrodes were rinsed with ultra-pure water to remove any unattached thiols. In order to ensure complete thiol coverage of the gold surface, the electrodes were backfilled for 1 h with 1 mM MCH prepared in 10 mM PB. Rinsing with ultra-pure water was then done, careful drying with a stream of nitrogen and placement in 10 mM PB for 1 h to stabilize the SAM before binding studies. Additionally, the micrux electrodes were also immersed in a blocking buffer (Thermo Scientific, USA) for 30 min. Before incubation of the PNA modified electrodes for 30 min, the 20 nM of the complementary ss-DNA target solution prepared in 10 mM PB was heated to 90 ℃ for 5 min. The ss-DNA sequence used is as follow 5'-AAA TTA TGA TTG TGA CGT AAT CCC AAT ACA ACG TCA ATG ACC TAC CGT T-3' (Sigma-Aldrich, UK). The electrodes were then carefully washed to remove non-specifically bound DNA and kept in PB for further use.

2.1.3   Investigation of the Intercalator-hybridized Probe Binding

To monitor the hybridization event, a ferrocene-based intercalator (University of Cardiff, UK) was employed and investigated its binding behaviour with the PNA-DNA duplex. To do so, the above hybridized electrodes were incubated with 55.57 µM intercalator for 30 min at room temperature. The resulting electrodes were carefully rinsed and measured in BioFET.

2.2   EIS measurements

2.2.1   Setup

Electrochemical measurements were performed using a CompactStat potentiostat (Ivium Technologies, The Netherlands) with a three-electrode cell setup consisting of a Ag/AgCl (saturated KCl) reference electrode (BASi, USA) connected via a salt bridge filled with 10 mM PB, a Pt counter electrode (ALS, Japan) and gold working electrodes (CH Instruments, USA). All measurements were performed at room temperature. Electrochemical impedance spectroscopy (EIS) was carried out in 10 mM PB containing 5 mM $K_4[Fe(CN)_6]$ (Potassium hexacyanoferrate (III)) and 5 mM $K_3[Fe(CN)_6]$ (Potassium hexacynoferrate(II) trihydrate). The impedance spectrum was measured over the frequency range 100 kHz to 100 MHz, with a 10 mV a.c. voltage superimposed on a d.c. bias of 0.195 V vs. Ag/AgCl, corresponding to the formal potential of the redox couple. The obtained impedance data was fitted in an equivalent circuit model using the IviumSoft. Ferrocene peaks were monitored using differential pulse voltammetry (DPV) in 10 mM PB as supporting electrolyte. DPV scans were monitored between - 0.4 V and 0.7 V or 0.5 vs. Ag/AgCl with a scan rate of 0.05 Vs^{-1}.

2.2.2   PNA-based Biosensor

Gold working electrodes with a diameter of 2.0 mm were cleaned using a protocol adapted from elsewhere (Jolly *et al.*, 2015; Gaiji *et al.*, 2017). The electrodes were first mechanically polished for 5 minutes with 50 nm alumina oxide particles (Sigma Aldrich, UK) on a polishing pad (Buehler) followed by rinsing with excess water and sonication in ultra-pure water for 10 minutes to remove any remaining residues. Chemical cleaning was applied where the electrodes were immersed in a freshly prepared piranha solution for 10 minutes and then rinsed with ultra-pure water. Thereafter, electrodes were electrochemically cleaned in a three-electrode cell configuration by immersing them in a 0.5 M H_2SO_4 solution (Sigma Aldrich, UK) and the potential was scanned between the oxidation and reduction potentials of gold, −0.05 V and +1.5 V vs. Ag/AgCl (concentrated KCl), with a scan rate of 0.2 Vs^{-1} for 50 cycles until no further changes in the voltammogram were noticed. Finally, the cleaned electrodes were thoroughly rinsed with ultra-pure water, dried and incubated with an immobilization solution for 16 h in a humidity chamber. The protocol used for the preparation of the immobilization solution was the same as described in section 2.1.3 as well as the following steps. The ratio between PNA and MCH was 1:29. Electrodes were also prepared only with MCH. The DNA hybridization study was investigated using EIS measurements following the same protocol as described in section 2.1.2. The investigation of the Intercalator-hybridized probe binding was applied as before in section 2.1.3 and analysed using DPV.

3 Results and Discussion

3.1 BioFET characterization of a PNA-DNA Intercalator

3.1.1 PNA-DNA Hybridization and blocking buffer

The performance of a biosensor is directly related to the success of the different fabrication steps. One of the most relevant is the immobilization of the PNA probe on the gold electrodes and the hybridization. Thus, an initial study of the immobilization and following hybridization was done to ensure that the chosen ratio is able to provide the expected results. For this initial study, Micrux Technologies electrodes (referred to as micrux electrodes) were used and a PNA:MCH ratio of 1:29 was established. A blocking buffer was also applied to reduce non-specific biding. In the case of the BioFET used, as in Figure 3.1, a n-type transistor, when the gate-to-source voltage (V_{GS}) is altered, the conductivity of the channel is modulated and thereby I_D is altered.
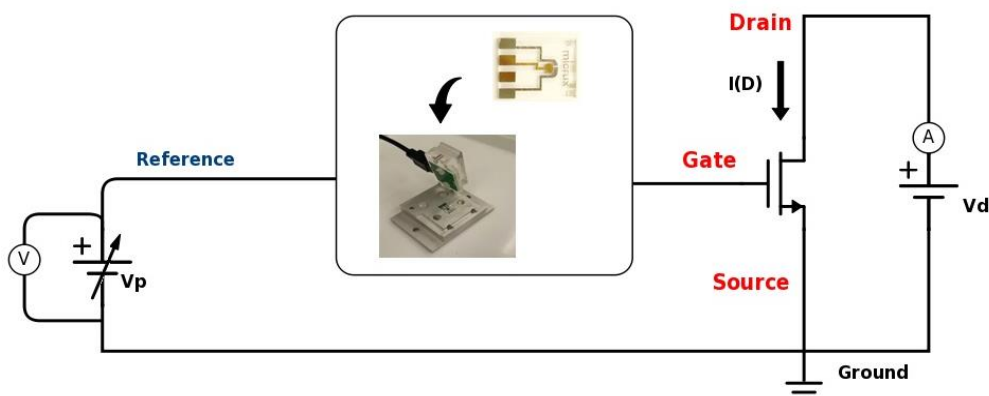
Figure 3.1 - Working principle of the BioFET sensor. A micrux electrode placed in a flow cell is connected to the gate of a MOSFET.

After DNA incubation and, thus, hybridization of the immobilized neutrally charged PNA probe with the negative charge target DNA occurs there is an increase in negative charge which causes a change in the interface surface dipole χ_{int} and the electrochemical double-layer potential ψ_{dl}. This causes a shift in the current–voltage (I–V) characteristic of the FET, more specifically a positive shift in the V_{GS} of the BioFET, as in the example in Figure 3.2.
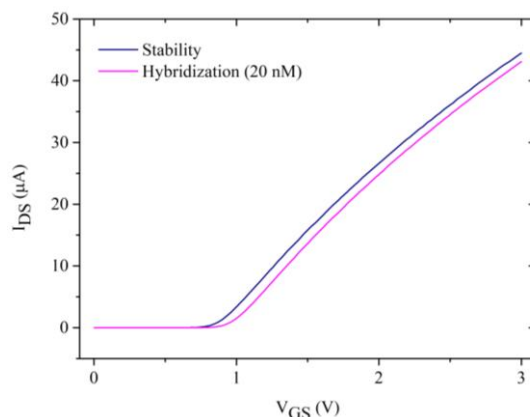
Figure 3.2 - BioFET I_D/V_{GS} characteristic of a PNA-DNA hybridization for an electrode before (Stability line) and after (Hybridization line) 20 nM DNA binding.

Therefore, based on what was previously described, it is possible to detect the hybridization event only by recording the shift in the I_D/V_{GS} curves. In order to obtain a better comparison between all of the data, a current of 0.25 μA was chosen to extract the V_{GS} values of all of the measurements.

In this initial study three separated days of measurements were recorded and on each day, results were obtained with and without the use of a blocking buffer. On each day new electrodes were used. The recorded shifts are shown in Figure 3.3.
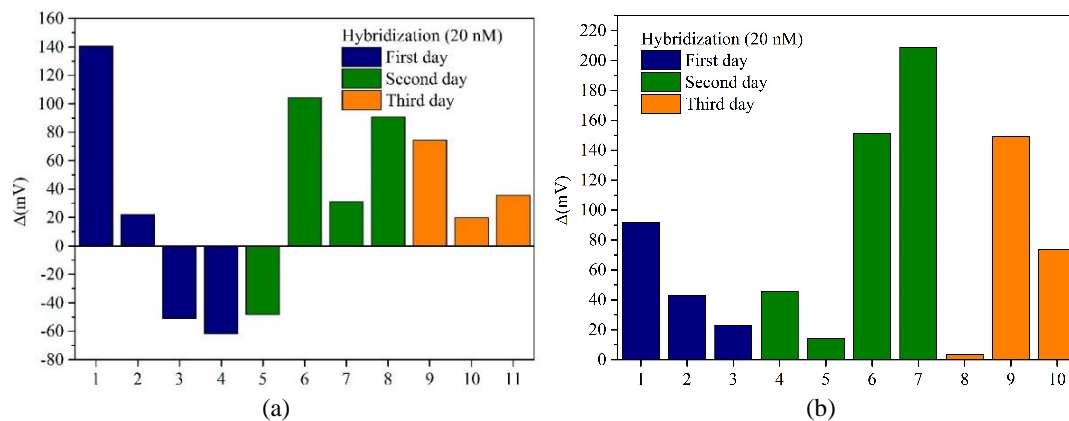
Figure 3.3 – BioFET PNA-DNA hybridization shifts obtained with a 1:29 ratio in different days (a) without a blocking buffer and (b) with a blocking buffer.

Before the addition of DNA for incubation, the electrode is immersed in 10 mM PB to stabilize the created SAM. During the stability period, the shifts between the stability curves are also measured so that a stable state is ensured and the last measurement performed is the one used for the detection of the hybridization. Typically, the SAM was considered stable when there was less than 10 mV of shift in between stability curves. Thus, for the purpose of the analyses of the obtained shifts after hybridization, 20 mV was established as the minimum shift to be considered as hybridization.

Taking that in consideration, a maximum value of 140.46 mV was obtained for hybridization without blocking buffer (Figure 3.3 (a)) and 208.63 mV for hybridization with blocking buffer (Figure 3.3 (b)).

It is of note, that in the electrodes where a blocking buffer was used, only positive shifts were recorded. However, in some results, as the shifts are quite low, no hybridization or almost none occurred. This might indicate some problems with the thiolation process of the used PNA or even with the DNA, as it might not have been handled properly, in a clean environment or even affected by desoxirribonuclease (DNAse), for example. The average shifts were also calculated and the obtained results can be seen in Figure 3.4.

(a)   (b)
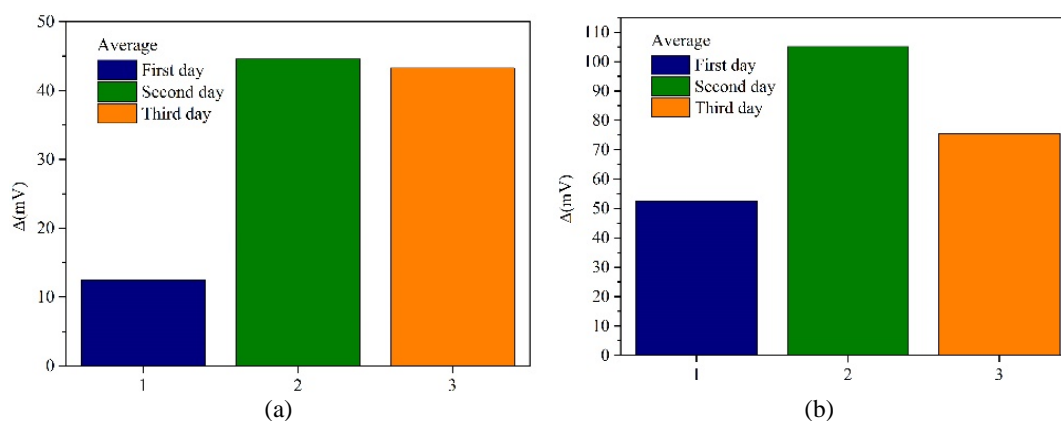
Figure 3.4 – Average of the hybridization shifts from Figure 3.3, in which (a) is without a blocking buffer and (b) with a blocking buffer.

Comparing the 2 set of results, it can be seen that the average shift caused by the DNA hybridization with a blocking buffer is higher than the one without. A maximum average hybridization shift of 44.55 mV was obtained for Figure 3.4 (a), in which no blocking buffer was used. In contrast with the 105.074 mV average shift obtained with the use of a blocking buffer.

However, as the blocking buffer has proteins, which is unknown what they are. These proteins could be up just a few nm in size but they could also not be as few as expected which will definitely hinder the binding of the DNA to the lower part of the PNA. Thus, it was considered that the use of the blocking buffer could interfere with the formation of PNA-DNA duplexes and, thus, might interfere with the binding of the intercalator, being chosen to not continuing with the use of the blocking agent.

3.2   Characterization of the Intercalator-hybridized Probe Binding

In order to demonstrate the interaction between the intercalator and the PNA-DNA duplexes, BioFET was used to monitor the changes in the I_D/V_{GS} curves before and after incubation with the intercalator. In this work, a ferrocene-based intercalator, which a structural formula as Figure 3.5, was used.
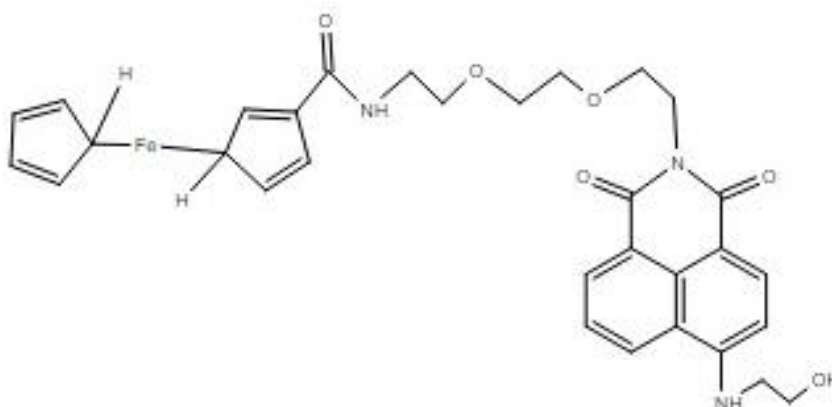
Figure 3.5 – Structural formula of the ferrocene-based intercalator used.

It was theorized that with the addition of this intercalator, which binds in between adjacent base pairs of the PNA-DNA duplex, an increase of the negative charge density would occur and thus produce a positive shift in the I_D/V_{GS} curves, as in Figure 3.6.
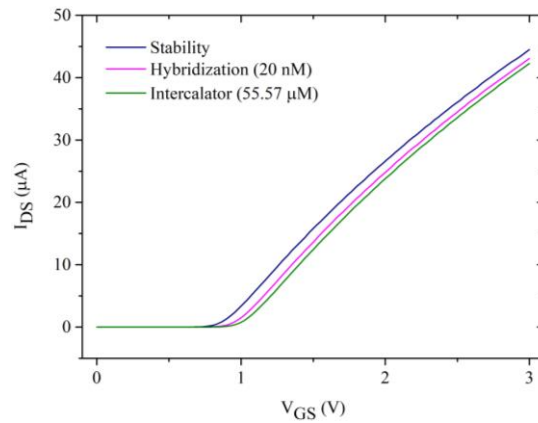
Figure 3.6 - BioFET I_D/V_{GS} characteristic for an electrode before (Stability line), after 20 nM DNA binding (Hybridization line) and after 55.57 µM of intercalator binding (Intercalator line).

Following the hybridization DNA study done before, a PNA:MCH ratio of 1:29 was also used. In Figure 3.7 the shifts measured in two separated days are shown.
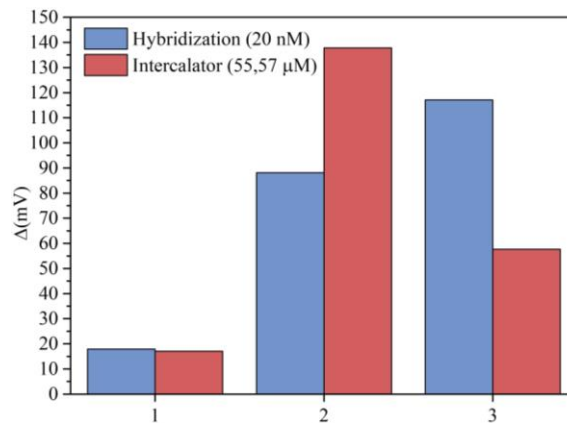
Figure 3.7 - BioFET PNA-DNA hybridization and intercalator shifts with a PNA:MCH ratio of 1:29 obtained in different days (1 and 2 in one day and 3 in another).

A positive shift of 137.78 mV was achieved in 2 of Figure 3.7. However, all of the other shifts are smaller than the one measured after hybridization. In the case of the hybridization shift 1, a hybridization shift of less than 20 mV was obtained but the intercalator was still tested. Yet, the low hybridization shift might indicate that no hybridization occurred or only a very small percentage of it, so it was expected that the intercalator wouldn't cause a positive shift since without PNA-DNA duplexes the intercalator wouldn't have a place to bind. Nevertheless, in the case of 3 a large hybridization shift can be observed and the intercalator shift was smaller.

In Figure 3.8, the average of the shift is calculated for both days.
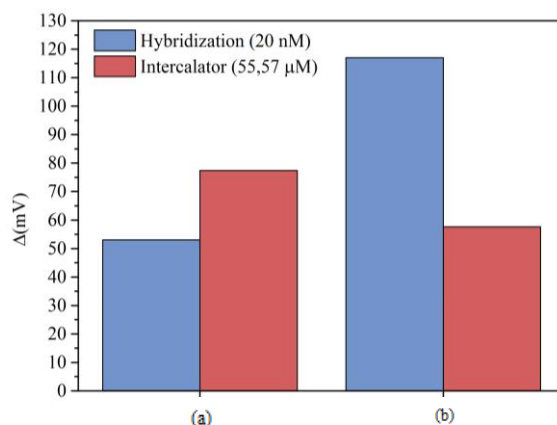
Figure 3.8 - Average of shifts from Figure 3.7, in which (a) represents the average of 1 and 2 and (b) represents 3.

It can be noticed that even though the hybridization shift in (b) is larger than the one in (a), the shift caused due to the intercalator is larger in (a). It was argued that the use of a high PNA:MCH ratio was one of the possible reasons for this occurrence, as such a high ratio would mean that the PNA probe surface density would be low and it would decrease the hybridization yield and consequently the binding of the intercalator. For the purpose of exploring this possibility a 1:19 ratio was tried out. The results of the measurements performed are depicted in Figure 3.9.
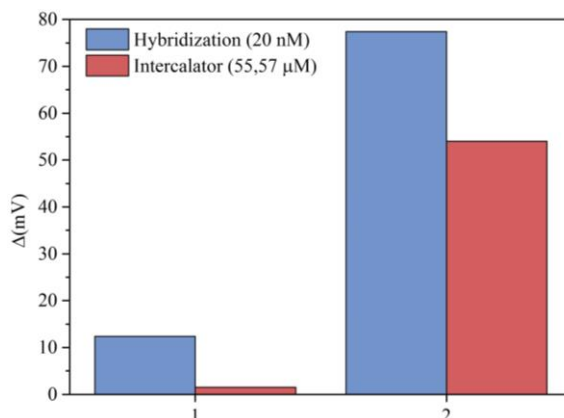
Figure 3.9 - BioFET PNA-DNA hybridization and intercalator shifts with a PNA:MCH ratio of 1:19 obtained in one day.

As it can be observed in shift 1 of Figure 3.9, a hybridization shift of less than 20 mV was obtained and as before a negative intercalator shift was measured. In the case of the shift 2 from the same figure, even though there was a 77.4 mV hybridization shift, no positive shift was gotten after the intercalator.

In Figure 3.10, it is displayed an average of the shifts obtained for both ratios, 1:29 and 1:19.
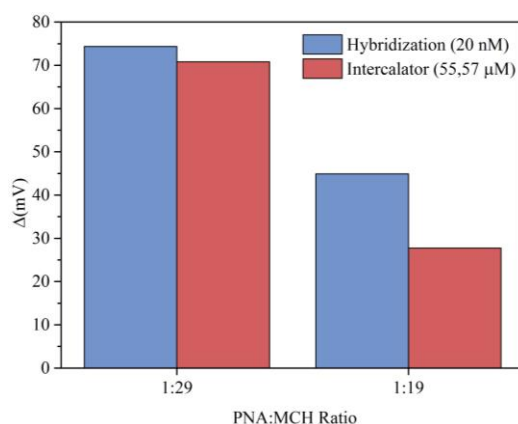
Figure 3.10 - Average of the hybridization shifts obtained for the PNA:MCH ratios of 1:29 and 1:19.

In average, in spite of what was theorized, both ratios did not produce a positive shift of the intercalator, even though both had a high hybridization shift. It can be deduced that either the hypothesis announced before might not be correct or the intercalator is not providing the proper results, as only one positive result was achieved and it was not reproducible.

To prove if either of this is true, EIS was used to measure the changes in impedance of the system as a result of hybridization and DPV to monitor the significance of the intercalator to generate an electrochemical response related to the PNA-DNA hybridization.

3.2.1 EIS Characterization of DNA Hybridization

EIS in Faradaic mode, in which redox probes are used, was applied in this study to analyse the changes on the charge transfer resistance of the system at the electrode/electrolyte interface as a result of the binding event. Such technique was chosen since it can provide valuable qualitative and quantitative information about the electrical double layer at the sensor interface and also understanding of the electrochemical behaviour of the system, even if the changes in impedance depend on many factors. One of the biggest advantages of EIS is the possibility to differentiate the different phenomena happening at the electrochemical double layer, for instance the charge transfer, the diffusion transport or the double layer formation.

For the electrochemical characterization, a ratio of 1:29 was applied, since it was the ratio optimized for this technique in experiments previously performed by the group and the one that was tested during the initial study. The electrodes were initially stabilized in 10 mM PB before conducting binding experiments. For binding, a 100 nM DNA concentration was applied so that the modified surface of the old electrodes is saturated and the maximum PNA-DNA duplexes are formed. Electrodes with no DNA incubation were also tested, so that control results would be obtained.

Figure 3.311 shows a nyquist plot of a typical EIS behaviour of the PNA / MCH immobilized gold electrode in the presence of ferri/ferrocyanide.

(a)	(b)
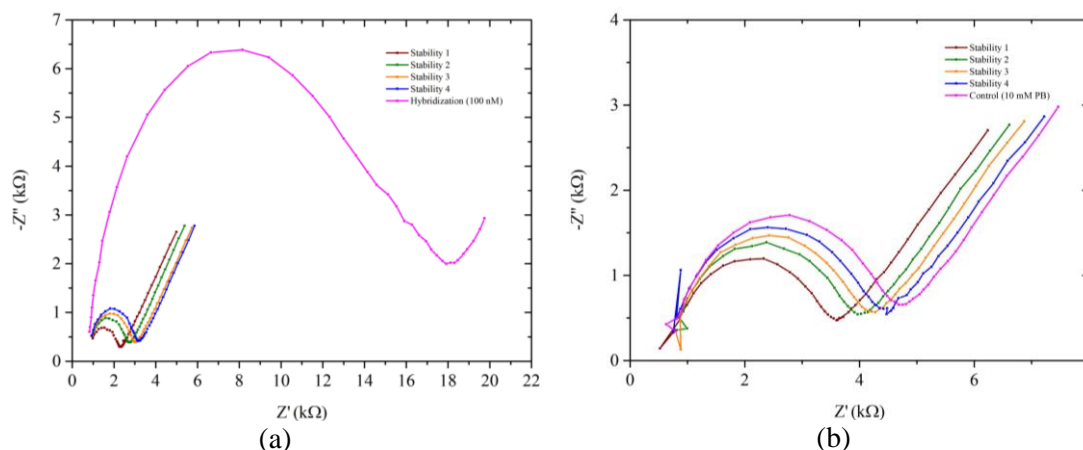
Figure 3.11 – Nyquist plots of a 1:29 ratio PNA/MCH immobilized gold electrode, (a) before and after incubation with 100 nM complementary ssDNA and (b) without hybridization.

In an impedance measurement, the typical Nyquist plot obtained (Figure 3.11) usually include a semicircle region lying on the axis followed by a straight line. The semicircle portion (at higher frequencies) corresponds to the electron-transfer-limited process, and the straight line (at low-frequency range) represents the diffusion-limited electron transfer process (Estrela and Migliorato, 2007).

The charge transfer resistance (Rct) was determined by fitting data to a modified Randles equivalent circuit (Figure 3.12) has been replaced by a constant phase element (CPE) (Keighley *et al.*, 2008). CPE is used instead of a pure capacity since it takes into account the topological imperfections of the biolayer on the surface of the electrode and a better fitting is obtained. CP is given by:

$$Z = A(j\omega)^{-n} \tag{2}$$

,where *A* and n are experimental parameters ($0 \leq n \leq 1$). Depending on n, three special cases can be considered: if n = 0, *Z* represents an ideal resistance and *A* = *R*; if n = 1, then *Z* corresponds to an ideal capacitor where *A* = 1/*C*, and if n = 0.5, the circuit element is termed the Warburg impedance, where *A* = *W* (Maalouf *et al.*, 2007).
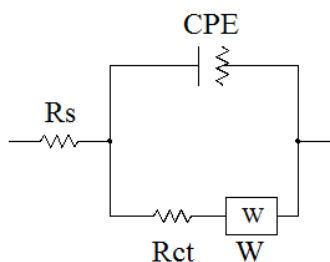
Figure 3.12 - Equivalent electrical circuit diagram used to fit the impedance spectra.

The equivalent circuit consists of the following elements: the resistance of the solution Rs and the CPE in parallel with Rct and the Warburg element (W), which models the diffusion of redox couple.

For the purpose of the analysis of the changes caused by hybridization, only the fitted values obtained for Rct will be presented (Figure 3.13). However, fittings of the other elements were also obtained and are presented in the Appendice B.
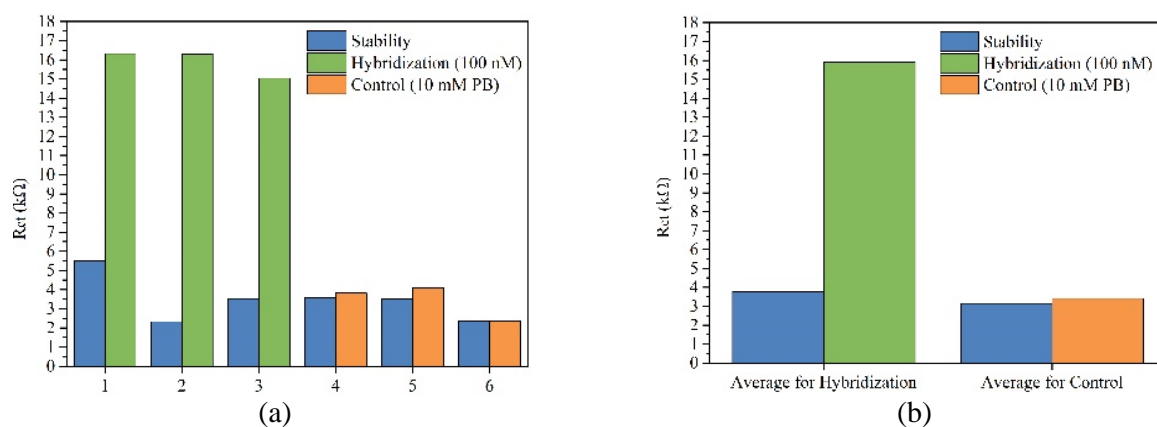
Figure 3.13 – Obtained fitting values for Rct for before and after incubation (a) three electrodes with 100 nM DNA hybridization and three without DNA (control) and (b) the average for each.

From Figure 3.13 (a), the relatively neutral PNA-MCH monolayer, represented by the stability column, shows a relatively small Rct for all of the tested electrodes. In the Figure 3.13 (b), the average Rct before incubation for the three electrodes was 3.789 kΩ and for the control 3.151 kΩ. These values can be attributed to the neutral PNA molecules demonstrating a physical barrier to the negatively charged markers. After hybridization with the complementary DNA sequence, an increase of Rct can be observed in Figure 3.13 (a), where there is a notorious difference between the Rct obtained for hybridization and for control. This augmentation could be associated to an increased electrostatic barrier to the negatively charged redox couple $[Fe(CN)_6]^{3-/4-}$ due to the negatively charged attached DNA (Mateo-Mart and Pradier, 2010).

To allow a better understanding of the changes during the stability period and after incubation, the average difference between stabilities and the difference between the last stability and hybridization was calculated (Figure 3.14).
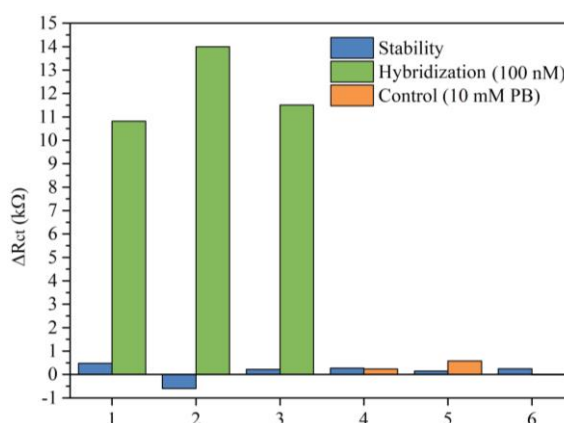
Figure 3.14 – Calculated variation of Rct where stability is the average difference between stabilities, hybridization and control are the difference between the stable state and after incubation.

As it was expected, the variation in between stabilities was quite low and so was the variation for the control. In average, the enhancement of Rct obtained for the control was 0.043 kΩ. After incubation

with 20 nM DNA there a higher difference was achieved and in average the enhancement was 12.07 kΩ.

3.2.2 DPV Characterization of Intercalator

Following the demonstration that hybridization occurs, the hybridized electrodes were incubated with the ferrocene-based intercalator and subjected to a DPV measurement. In this technique, the cell current is measured as a function of time and as a function of potential. The potential is varied using pulses of increasing amplitude and the current is sampled before and after each application of the pulse. The difference between current measurements at these points for each pulse is determined. For potentials much higher than the redox potential, there is no faradaic reaction in response to the pulse, so the difference current is zero. At potential around the redox potential, the difference current reaches a maximum, and decreases to zero as the current becomes diffusion controlled.

Therefore, the resulting voltammogram displays the sampled current on the vertical axis and the potential to which the pulse is stepped on the horizontal axis. In Figure 3.15, it is shown the voltammograms obtained for the electrodes 2 and 5, from the previous hybridization.
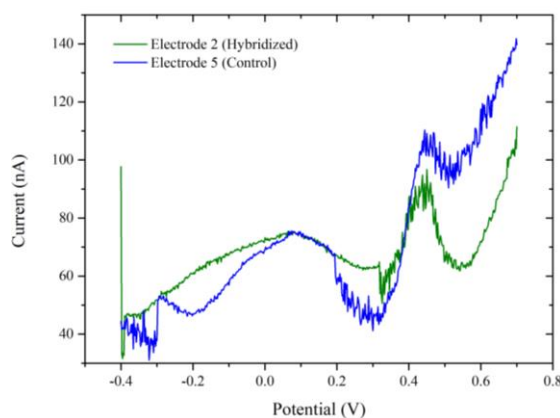
Figure 3.15 - DPV curve of 55.57 µM intercalator for the detection of PNA/DNA duplexes and the current as the function of the complementary DNA concentration.

Comparing the DPV voltammograms of the intercalator in the presence and the absence of complementary DNA, it confirms that the intercalator is not working as it was expected, since the peak current is not attributed to the hybridization phenomenon. This also proves a that there is not a significant interaction between the PNA/DNA duplex and the DNA intercalator. In order to confirm whether the intercalator is the problem, three bare electrodes, i.e. in which there is no immobilization solution and no DNA incubation, were used to perform DPV in the intercalator diluted in 10 mM PB (Figure 3.16).
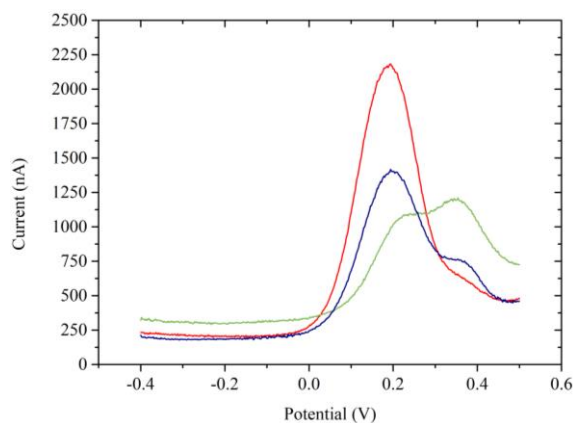
Figure 3.16 - DPV voltammograms of 55.57 µM intercalator diluted in 10 mM PB with blank electrodes.

A well-defined peak was expected to appear which would correspond to the oxidation of the ferro-cene moieties. In the he voltammogram presented in red the well-defined peak was obtained and appears at about 0.2 V vs. Ag/AgCl, while in the others that doesn't happen as clearly. In the case of the volt-ammogram presented in green, it is quite noticeable that there are two peaks, the first is the same as the other curves and the second is also presented in the blue curve and there's a very small contribution in the red curve as well. Therefore, there are two peaks, one could be for the intercalator by itself and the other might be due to aggregates of the intercalator. These aggregates could have been formed due to the insolubility of the intercalator and could have a different oxidation potential. Consequently, the in-tercalator is not stable and thus will not provide results that are reliable and reproducible.

3.3   BioFET Optimization of PNA:MCH ratio

3.3.1   PNA-DNA Hybridization with Micrux Technologies Electrodes

The PNA:MCH ratio of 1:29, widely used throughout the experiments is the optimized ratio for application EIS but it still has to be optimized for use in BioFET. Ideally the optimized ratio would be the one with optimal density, corresponding to the biggest shift in the I_D/V_{GS} curves upon hybridization with target DNA. As a starting point for the optimization studies, it was considered that a higher density of PNA probe on the surface would increase the shift caused by hybridization since there would be more PNA to hybridize with the DNA and therefore more PNA-DNA duplexes would be created. In order to increase the density of the probe, the amount of MCH would have to decrease which would correspond to a decrease in the ratio. However, since the 1:29 ratio was previously optimized for EIS, it will continue to be used as a comparison term. As such, all shifts recorded for the 1:29 ratio, including all those obtained in the initial study without the use of a blocking agent and during the application of the inter-calator, as well as the average obtained on each day of measurements, will be shown in Figure 3.17.
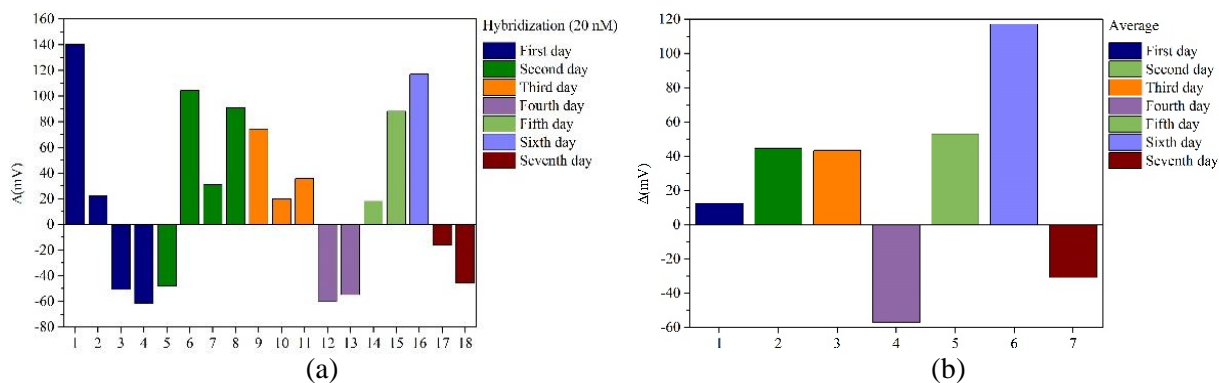
Figure 3.17 - BioFET PNA-DNA hybridization shifts obtained with a 1:29 ratio obtained in different days (a) and (b) the average for each day.

The analysis for the first recorded shifts (first, second and third day in the Figure 3.17 (a)) has been done previously in the initial study (section 3.11). The fourth, fifth and sixth were also analysed before during the application of the intercalator in section 0. In the 7th day, no hybridization was obtained and this may have been due to the temperature, since all measurements are done at the temperature of the room, which is not controlled. It was then stipulated that the next measures to be carried out would be at a set ambient temperature of 23 ° C. Looking at the average obtained for each day, it was calculated a maximum of 117.06 mV. As the goal is to decrease the ratio, a ratio of 1:19 was tested, which had been previously used during the application of the intercalator and was repeated again. The obtained shifts can be seen in Figure 3.18, as well as the average for both days. A ratio of 1:09 was also tried for the first time and the resulting shifts and average are shown in Figure 3.19.
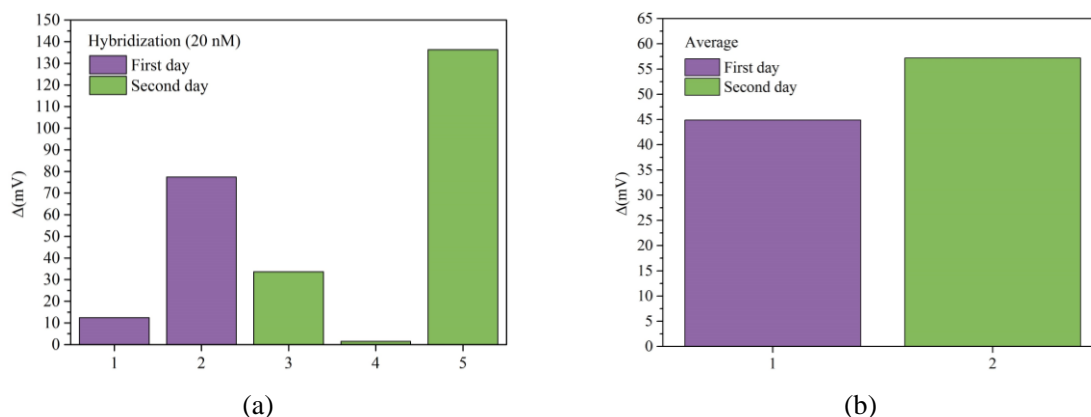
Figure 3.18 - BioFET PNA-DNA hybridization shifts obtained with a 1:19 ratio (a) in different days and (b) the average for each day.

(a)   (b)
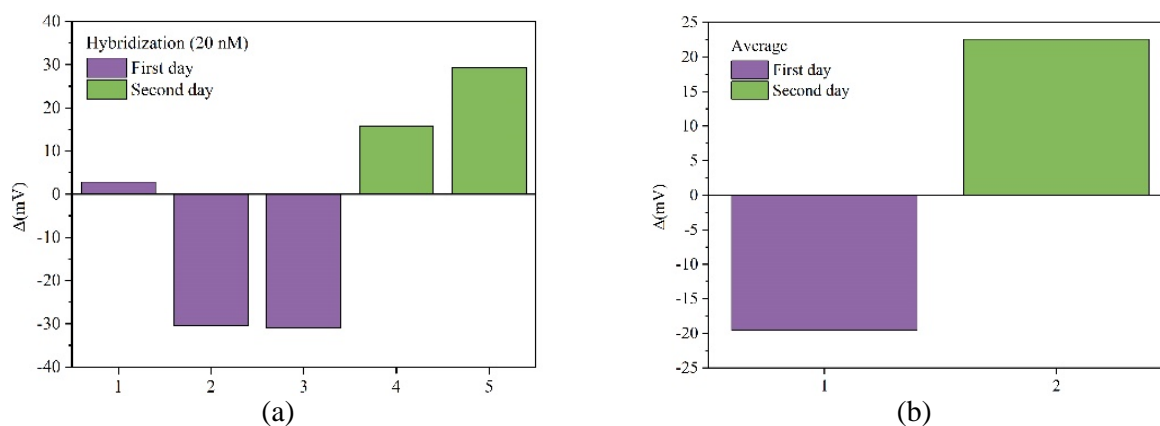
Figure 3.19 - BioFET PNA-DNA hybridization shifts obtained with a 1:09 ratio (a) in different days and (b) the average for each day.

Both ratios, above shown, were tried out in 2 days. In the case of 1:19 ratio, the first day corresponds to the hybridization shifts measured before the use of the intercalator (Section 3.2) and was previously commented. In the second day, it was measured the maximum value obtained for this ratio of 136.3 mV, yet it was also obtained a shift near 0 which might indicate that such high value might be due to unspecific binding, which means that more measurements should be done in order to confirm whether that maximum value can be replicated or it was indeed unspecific binding. The calculated average for each day of measurements was positive for both days and the maximum calculated was 57.16 mV. For 1:09 ratio, the first day it was tried out it was unsuccessful, not having been obtained a positive shift. In the second, positive results were obtained but only one was higher than 20 mV.

Until now, whenever BioFET measurements were done Micrux Technologies electrodes were used. However, due to the finish of the batch of new electrodes that have been used up and in order to reduce costs, the electrodes previously used were subjected to chemical cleaning. For this, they were immersed in a piranha solution (3 parts of concentrated H_2SO_4 with 1 part of H_2O_2) for 5 min, followed by UV-light for 10 min and the same cleaning done for new electrodes. The resulting cleaned electrodes were subjected to an immobilization solution with a ration of 1:29, as it is the one where the must results were obtained become easier to compare the recorded shifts. However, it was concluded that in electrodes cleaned with piranha solution it was not possible to obtain a stable SAM and so no reasonable hybridization shifts. As such, evaporated electrodes were suggested as an alternative. As a conclusion to the use of the Micrux Technologies electrodes, the following figure (Figure 3.20) shows the average obtained for the ratios 1:29, 1:19 and 1:09.
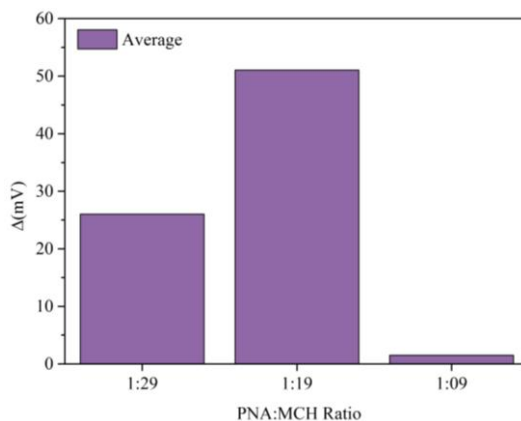
Figure 3.20 - Average of the all of the shifts obtained for the 1:29, 1:19 and 1:09 ratios.

The ratio in which was calculated the maximum average hybridization shift was 1:19, in which a shift of 51.03 mV was achieved. The average shift obtained for the 1:29 ratio was 26.02 mV and 1.51 mV for 1:09. Comparing the shifts, it can be deduced that the ratio 1:19 was the one to achieve a higher shift but in order to confirm its reproducibility more results would be needed. Also, the use of lower ratios such as 1:05, previously applied in PNA-DNA hybridizations in EIS, 1:03 and 1:04 should be tried out.

3.3.2 PNA-DNA Hybridization with Evaporated Electrodes

As said before, the use of the evaporated electrodes came from the need of finding another option to Micrux Technologies electrodes. These evaporated electrodes are gold array on a glass slide and each glass slide can have at least 8 gold electrodes. To obtain a mean of comparison between all of the ratios previously obtained it was planned to begin the optimization study with a 1:29 ratio (Figure 3.21).

(a) (b)
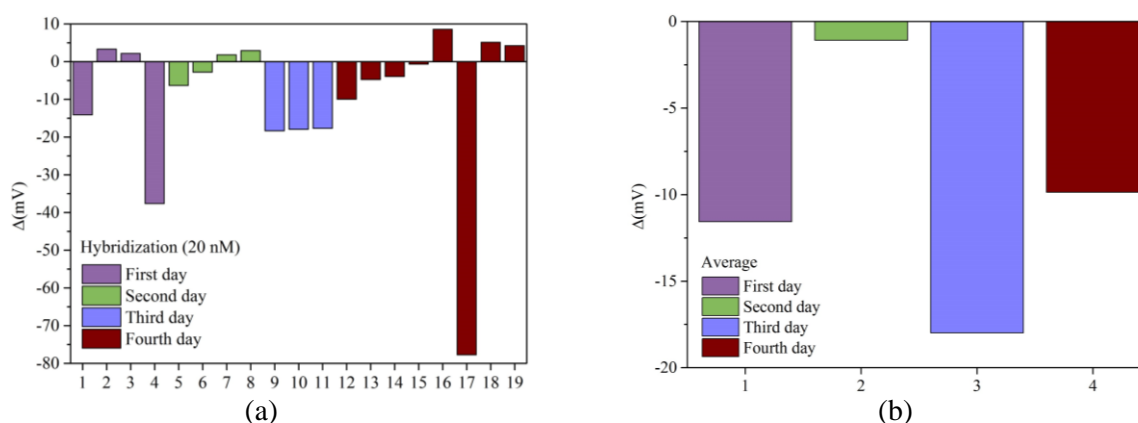
Figure 3.21 - BioFET PNA-DNA hybridization shifts with the use of evaporated electrodes obtained with a 1:29 ratio (a) in different days and (b) the average for each day.

Firstly, it is possible to observe that in any of the days it was possible to obtain shifts higher than 10 mV (Figure 3.21 (a)), most of which were negative shifts as is evident in the calculated average for each day, in Figure 3.21 (b). It is noteworthy that for each day different electrodes were used, since as they were electrodes fabricated by evaporation they would not resist chemical cleaning processes, such as the piranha solution that has been used. Furthermore, the application of UV-light was done after the first day of measurements as it was thought that the surface was hydrophobic and also would provide a better cleaning. In the case of the second day, it was thought that the negative results were due to the use of old electrodes, so before the third day, more electrodes were fabricated. However, a fabrication error occurred and the electrodes were not evaporated properly, not fitting as they should in the flow cell. Afterwards, another issue related to the flow cell was found, as the flow cells that have been used in the previous days was found to be too small and was covering the gold electrodes in the glass surface. For that reason, in the last day of tests a flow cell was manually created, as in Figure 3.22.
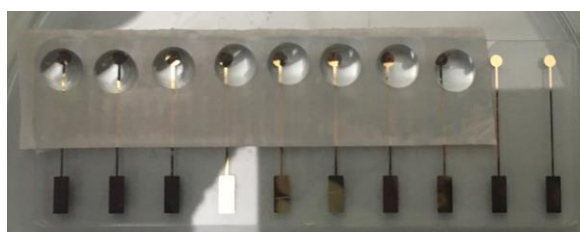
Figure 3.22 - Fabricated evaporated electrode with the manually created flow cell.

Nevertheless, no improvement was seen and thus characterization was performed in EIS to determine if not obtaining positive shifts, and therefore hybridization, is due to the electrodes.

3.3.2.1   EIS Characterization of PNA-DNA Hybridization

As previously stated, EIS was performed with the use of evaporated electrodes and a ratio of 1:29. After obtaining the impedance spectrum, such as in the example of Figure 3.23, a fitting of the impedance data was done using the equivalent electric circuit (Figure 3.12) and the obtained Rct values as well as the variation of Rct are shown in Figure 3.24.
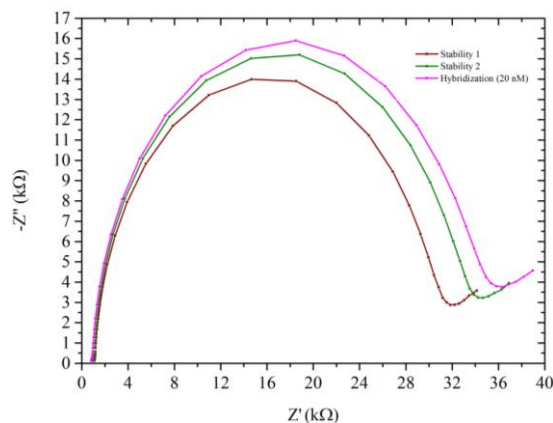
Figure 3.23 – Nyquist plot of an example of the impendence spectra obtained for the characterization of the PNA-DNA hybridization with a 1:29 ratio PNA/MCH evaporated gold electrode with 20 nM DNA.
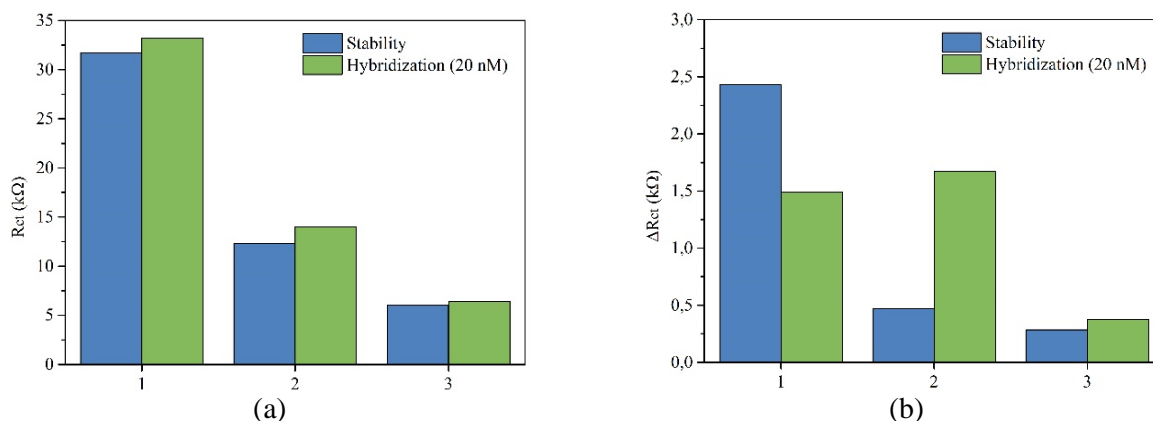
Figure 3.24 - (a) Fitting values of Rct obtained for an evaporated electrode before and after incubation with 20 nM DNA and (b) the variation of Rct, where stability is the difference between stabilities and hybridization, the difference between the stable state and after incubation.

As it can be seen from Figure 3.24 (a), hybridization appears to have been achieved. However, observing 1 in Figure 3.24 (b), it is possible to verify that although Rct increased in this electrode after hybridization, the difference is smaller than the difference between the stabilities, which leads to believe that, even though there was an increase in Rct after the incubation period, no hybridization occurred. In the case of electrode 2, this does not happen but the calculated variation after incubation is only slightly higher than the one obtained between stabilities, contrary to what has happened before. In electrode 3, this variation is almost the same and its behaviour resembles the one obtained for the control electrodes tested in section 3.2.1. Also in the same experiment, as previously mentioned, an average enhancement of 12.07 kΩ of Rct was obtained, for the same ratio, but with 100 nM ss-DNA and with the use of gold working electrodes. In this case, an average enhancement of 1,17 kΩ was achieved. Therefore, this might indicate that evaporated electrodes are unsuitable for this type of application. However, as new

DNA samples were ordered, with the same sequence, and used in this experiment it was necessary to verify if the ordered samples would provide a higher variation with the use of gold working electrodes in EIS instead of the evaporated ones.

3.3.3   EIS Characterization of PNA-DNA Hybridization with gold working electrodes

As mentioned before, gold working electrodes were used to verify if the PNA and new DNA samples would provide higher Rct than the evaporated electrodes. A ratio of 1:29 was again used and 2 nM of ss-DNA followed by 20 nM instead of 100 nM in order to only vary the electrodes used. The Rct fittings were made using the equivalent electric circuit of Figure 3.12.

The fitting values obtained for Rct are presented in Figure 3.25 (a) and the variation of Rct in Figure 3.25 (b).

(a)   (b)
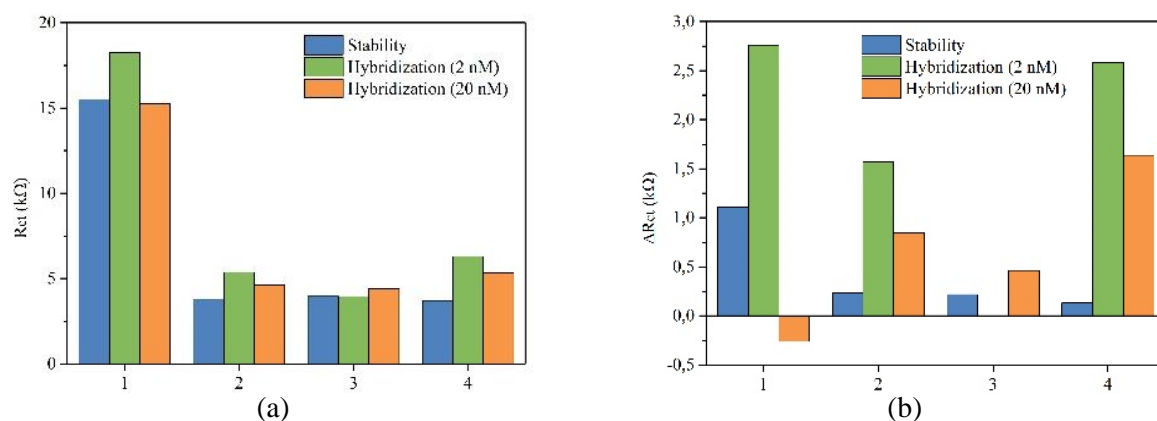
Figure 3.25 - (a) Fitting values of Rct for a gold working electrode and a 1:29 ratio obtained before after incubation with 2 and 20 nM DNA and (b) the variation of Rct, where stability is the difference between stabilities and hybridization the difference between the stable state and after incubation.

The values obtained are identical with each other, except for electrode 1, as shown Figure 3.25 (a), which demonstrates that obtaining low values will not be due to the electrodes used in these tests. Regarding the variation of Rct, the values obtained for 2 nM are similar to those obtained for the EIS of the evaporated electrodes. The average calculated for the variation when using 2 nM was 1.73 kΩ, while in the case of the evaporated electrodes it was 1.17 kΩ. Although in the case of these gold working electrodes the value of the Rct variation was higher compared to the difference between stabilities, these values remain very low. As such, several hypotheses were considered to explain this: the PNA used for the immobilization solution would be damaged and therefore would not be conveniently immobilized, since it is a batch of DNA different from the one previously used and even having the same sequence, the PNA-DNA combination may not be hybridizing sufficiently or at all, and this case the positive Rct variations are due to non-specific binding.

3.3.3.1   *EIS Characterization of MCH-DNA Hybridization*

In order to test if any of the hypotheses announced may be possible, EIS was performed using gold working electrodes and a 1:29 ratio but with an immobilization solution in which the PNA was replaced by 10 mM PB. In this way it may be possible to understand the interaction of the MCH with the incubated ss-DNA.

The Rct fittings were made using the equivalent electric circuit of Figure 3.12. The fitting values obtained for Rct are presented in Figure 3.26 (a) and the variation of Rct in Figure 3.26 (b).

(a)   (b)
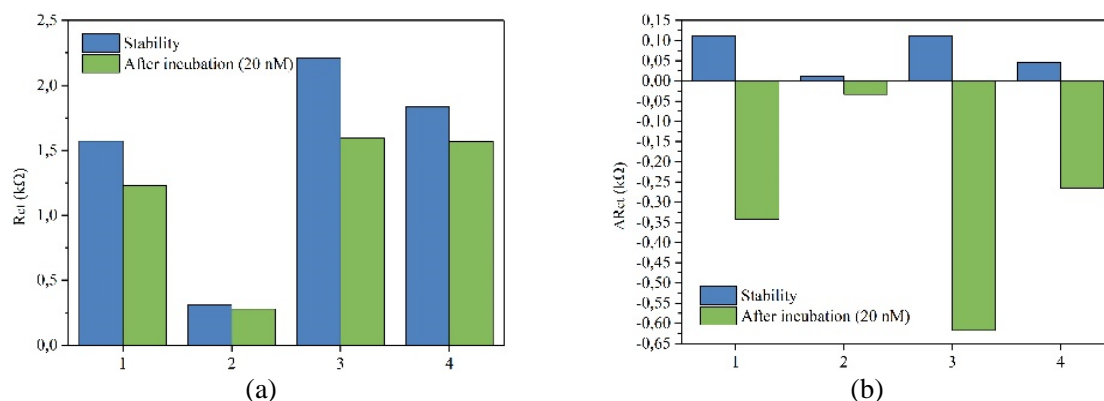
Figure 3.26 - (a) Fitting values of Rct for a gold working electrode, with a 1:29 ratio in which no PNA is in the immobilization solution, obtained before after incubation with 20 nM DNA and (b) the variation of Rct, where stability is the difference between stabilities and after incubation the difference between the stable state and after incubation.

By observing Figure 3.26 (a), it can be seen that, after incubation, Rct is lower than the stability state obtained prior to incubation. The same is confirmed by Figure 3.26 (b), where the variation after incubation is negative. Once the PNA was withdrawn from the immobilization solution, any positive variation in Rct would indicate that unspecific binding of the incubated ss-DNA would occur. As such is not the case, it is possible to exclude this hypothesis. However, this cannot serve as conclusive to determine that the reason for the low Rct variation comes from the PNA, since, it may be something related to the formation of SAM or to the formation of PNA-DNA duplexes or to the process which may be pulling out the hybridized ss-DNA.

4   Conclusion and Future Perspectives

The main goal of this thesis was the development of a BioFET biosensor based on the detection of PNA-DNA hybridization. To do so it was divided in two parts in which the several stages of the process were analysed:

Part one: Demonstration of BioFET detection of hybridization was achieved as well as a successful application of a blocking buffer. A maximum average hybridization shift of 44,55 mV was obtained without a blocking buffer in contrast with 105.07 mV obtained with a blocking buffer. Yet, it was concluded that further investigation must be done in order to understand if the results provided after the use of the blocking buffer are reliable and reproducible. For the application of the intercalator micrux electrodes were used and three PNA:MCH ratios were applied, 1:29, 1:19 and 1:09. However, with the use of EIS and DPV, the intercalator was proved to be unstable and insoluble and, thus, not reliable for the purposed application.

Part 2: Optimization of the PNA/MCH ratio and, thus, hybridization was investigated in BioFET. Again, micrux electrodes were used and ratios of 1:29, 1:19 and 1:09 were tried. For 1:29, an average shift of 26.02 mV was obtained, 51.03 mV for 1:19 and 1.51 mV for 1:09. In order to reduce costs, micux electrodes were replaced by evaporated electrodes. For a ratio of 1:29, no positive shifts were obtained with these type of electrodes, which might be due to temperature, fabrication and/or cleaning processes or they may not be usable for this application. Characterization of the PNA-DNA hybridization with EIS was done to verify if the electrodes were the issue. Additionally, gold working electrodes were used in EIS to ensure that the PNA-DNA combination was hybridizing. As the Rct values remained very low, it was necessary to understand if the changes in were caused by unspecific biding. So, EIS was done, using gold working electrodes and the same ratio, but without addition of PNA to the immobilisation solution. This experiment allowed to conclude that there is no unspecific interaction between the MCH and ss-DNA incubated.

Future perspectives in regards to this work include the continuation of the PNA/MCH ratio optimization in BioFET, as it has not been reported. Study of the influence of chemical cleaning times in the stability of the SAM in micrux technologies electrodes to allow reduction of costs. Additionally, search of new electrodes to allow better coverage and stability of the SAM whilst being cost efficient and reusable. Relatively to the hybridization process, test out the use of non-complementary DNA and real samples to study the influence of unspecific binding in the obtained hybridization shifts. Related to that, further investigation of the use of a blocking buffer should also be done as, although the results of its use might be a bit unreliable, good positive hybridization shifts were achieved, proving to be a good possibility for further investigation.

Furthermore, a miniaturization of the whole system could also be tried, by combining the electrochemical cell and the FET structure, allowing a smaller and more portable system.

5   References

Bala, A. and Gorski, L. (2016) 'Application of nucleic acid analogues as receptor layers for biosensors', *Analytical Methods*, 8(2), pp. 236–244. doi: 10.1039/c5ay02620b.

Bhalla, N. *et al.* (2016) 'Introduction to biosensors', *Essays in Biochemistry (2016)*, (June), pp. 1–8. doi: 10.1042/EBC20150001.

Clark, L. C. and Lyons, C. (1962) 'Electrode systems for continuous monitoring in cardiovascular surgery.', *Annals of the New York Academy of Sciences*, 102(1), pp. 29–45. doi: 10.1111/j.1749-6632.1962.tb13623.x.

Demidov, V. V *et al.* (1994) 'Stability of peptide nucleic acids in human serum and cellular extracts.', *Biochemical pharmacology*, 48(6), pp. 1310–3. Available at: http://www.ncbi.nlm.nih.gov/pubmed/7945427.

DeRisi, J. L., Iyer, V. R. and Brown, P. O. (1997) 'Exploring the Metabolic and Genetic Control of Gene Expression on a Genomic Scale', *Science*, 278(5338), pp. 680–686. doi: 10.1126/science.278.5338.680.

Egholm, M. *et al.* (1993) 'PNA hybridizes to complementary oligonucleotides obeying the Watson–Crick hydrogen-bonding rules', *Nature*, 365(6446), pp. 566–568. doi: 10.1038/365566a0.

Estrela, P. (2015) 'Molecular Analysis: BioFET Detection Sensors', in Sawan, M. (ed.) *Handbook of Biochips*. New York, NY: Springer New York, pp. 1–19. doi: 10.1007/978-1-4614-6623-9.

Estrela, P. and Migliorato, P. (2007) 'Chemical and biological sensors using polycrystalline silicon TFTs', *J. Mater. Chem.*, 17(3), pp. 219–224. doi: 10.1039/B612469K.

Gaiji, H. *et al.* (2017) 'A Peptide Nucleic Acid (PNA)-DNA Ferrocenyl Intercalator for Electrochemical Sensing', *Electroanalysis*, 29(3), pp. 917–922. doi: 10.1002/elan.201600576.

Gao, H. *et al.* (2011) 'Electrochemical deoxyribonucleic acid biosensor based on the self-assembly film with nanogold decorated on ionic liquid modified carbon paste electrode', *Analytica Chimica Acta*. Elsevier B.V., 704(1–2), pp. 133–138. doi: 10.1016/j.aca.2011.07.044.

Grieshaber, D. *et al.* (2008) 'Electrochemical Biosensors -Sensor Principles and Architectures', *Sensors*, 8(January), pp. 1400–1458. doi: 10.3390/s8031400.

Hammond, J. L. *et al.* (2016) 'Electrochemical biosensors and nanobiosensors', *Essays In Biochemistry*, 60(1), pp. 69–80. doi: 10.1042/EBC20150008.

Hosseini, S. M., Tavallaei, M. and Hosseini, E. (2015) 'A Review of Field-effect Transistors for Nucleic acid-based Medical Diagnosis', *Advances in Bioresearch*, 6(November), pp. 1–8. doi: 10.15515/abr.0976-4585.6.6.18.

Hyrup, B. and Nielsen, P. E. (1996) 'Peptide Nucleic Acids (PNA): Synthesis, Properties and Potential Applications', *Bioorganic & medicinal chemistry letters*, 4(1), pp. 5–23. doi: 10.1016/0968-0896(95)00171-9.

Jolly, P. *et al.* (2015) 'A simple and highly sensitive electrochemical platform for detection of MicroRNAs', *2015 IEEE SENSORS - Proceedings*, pp. 8–11. doi: 10.1109/ICSENS.2015.7370378.

Keighley, S. D. *et al.* (2008) 'Optimization of label-free DNA detection with electrochemical impedance spectroscopy using PNA probes', *Biosensors and Bioelectronics*, 24(4), pp. 906–911. doi: 10.1016/j.bios.2008.07.041.

Lisdat, F. and Schäfer, D. (2008) 'The use of electrochemical impedance spectroscopy for biosensing', *Analytical and Bioanalytical Chemistry*, 391(5), pp. 1555–1567. doi: 10.1007/s00216-008-1970-7.

Lorenz, W. and Schulze, K. D. (1975) 'Application of transform-impedance spectrometry.', *Journal of Electroanalytical Chemistry*, 65(1), pp. 141–153.

Lowe, C. R. (2008) 'Overview of Biosensor and Bioarray Technologies', *Handbook of Biosensors and Biochips*, p. 16. doi: 10.1002/9780470061565.hbb003.

Maalouf, R. *et al.* (2007) 'Label-Free Detection of Bacteria by Electrochemical Impedance Spectroscopy: Comparison to Surface Plasmon Resonance', *Analytical Chemistry*, 79(13), pp. 4879–4886. doi: 10.1021/ac070085n.

Mateo-Mart, E. and Pradier, C.-M. (2010) 'A Novel Type of Nucleic Acid-based Biosensors: the Use of PNA

Probes, Associated with Surface Science and Electrochemical Detection Techniques', in *Intelligent and Biosensors*. InTech, pp. 323–344. doi: 10.5772/7160.

Mohanty, S. P. and Koucianos, E. (2006) 'Biosensors: A tutorial review', *IEEE Potentials*, 25(2), pp. 35–40. doi: 10.1109/MP.2006.1649009.

Nielsen, P. E. *et al.* (1991) 'Sequence-selective recognition of DNA by strand displacement with a thymine-substituted polyamide.', *Science (New York, N.Y.)*, 254(5037), pp. 1497–1500. doi: 10.1126/science.1962210.

Pachauri, V. and Ingebrandt, S. (2016) 'Biologically sensitive field-effect transistors: from ISFETs to NanoFETs', *Essays In Biochemistry*, 60(1), pp. 81–90. doi: 10.1042/EBC20150009.

Paleček, E. and Bartošík, M. (2012) 'Electrochemistry of nucleic acids', *Chemical Reviews*, 112(6), pp. 3427–3481. doi: 10.1021/cr200303p.

Ray, A. and Nordén, B. (2000) 'Peptide nucleic acid (PNA): its medical and biotechnical applications and promise for the future.', *FASEB journal : official publication of the Federation of American Societies for Experimental Biology*, 14(9), pp. 1041–60. doi: 14(9),1041-1060.

Ronkainen, N. J., Halsallb, H. B. and Heinemanb, W. R. (2010) 'Electrochemical biosensors', *Chemical Society Reviews*, 39, pp. 1747–1763. doi: 10.1039/b714449k.

Schöning, M. J. and Poghossian, A. (2002) 'Recent advances in biologically sensitive field-effect transistors (BioFETs).', *The Analyst*, 127(9), pp. 1137–1151. doi: 10.1039/b204444g.

Schöning, M. J. and Poghossian, A. (2006) 'Bio FEDs (Field-Effect Devices): State-of-the-art and new directions', *Electroanalysis*, 18(19–20), pp. 1893–1900. doi: 10.1002/elan.200603609.

Takenaka, S. *et al.* (2000) 'DNA sensing on a DNA probe-modified electrode using ferrocenylnaphthalene diimide as the electrochemically active ligand', *Analytical Chemistry*, 72(6), pp. 1334–1341. doi: 10.1021/ac991031j.

Thévenot, D. R. *et al.* (2001) 'Electrochemical biosensors: Recommended definitions and classification', *Biosensors and Bioelectronics*, 16(1–2), pp. 121–131. doi: 10.1016/S0956-5663(01)00115-4.

Vo-Dinh, T. and Cullum, B. (2008) 'Biosensors and biochips: advances in biological and medical diagnostics.', *Fresenius' journal of analytical chemistry*, 366(6–7), pp. 540–551. doi: 10.1007/s002160051549.

Wang, J. (1998) 'DNA biosensors based on peptide nucleic acid (PNA) recognition layers. A review', *Biosensors and Bioelectronics*, 13(7–8), pp. 757–762. doi: 10.1016/S0956-5663(98)00039-6.

Wang, J. (1998) 'PNA biosensors for PNA Acid detection', *Current Issues Molec. Biol*, 1(2), pp. 117–122.

Wang, J. and Kawde, A. N. (2001) 'Pencil-based renewable biosensor for label-free electrochemical detection of DNA hybridization', *Analytica Chimica Acta*, 431(2), pp. 219–224. doi: 10.1016/S0003-2670(00)01318-0.

Wang, K. *et al.* (2011) 'Design of a sandwich-mode amperometric biosensor for detection of PML/RARα fusion gene using locked nucleic acids on gold electrode', *Biosensors and Bioelectronics*. Elsevier B.V., 26(6), pp. 2870–2876. doi: 10.1016/j.bios.2010.11.030.

Yang, Z. *et al.* (2015) 'A novel DNA biosensor using a ferrocenyl intercalator applied to the potential detection of human population biomarkers in wastewater', *Environmental Science and Technology*, 49(9), pp. 5609–5617. doi: 10.1021/acs.est.5b00637.

Appendices

A. BioFET electrodes and set up

1. Electrodes

Thin-film double metal-based single electrodes with 10×6×0.75 mm in dimensions. Three-electrodes approach: gold working electrode (1 mm of diameter), platinum reference and platinum counter electrode.
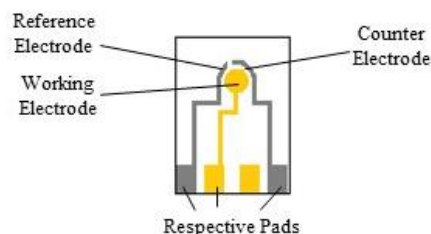
Figure A.1 - Micrux Technologies electrode.

Evaporated gold electrodes with arrays of gold electrodes with 2 mm in diameter. Prepared in-house on glass slides, with 75×26×1 mm in dimensions, using a thermal evaporator (BOC Edwards, UK). The glass slides were firstly exposed to chemical cleaning using piranha solution (H_2SO_4/ H_2O_2, v/v 3/1) for 10 minutes. The process, performed under fine vacuum (2.0×10^{-6} mbar), consists of an initial evaporation of 10 nm of chromium through a shadow mask followed by 150 nm of gold. Chromium was used as an intermediate layer since gold does not naturally adhere to glass.

2. Set up
- Flow cells

In order to connect the electrodes to the FET structure and the semiconductor device analyser, two flow cells, correspondent to the two types of electrodes, had to be used.

In the case of the micrux electrodes an all-in-one cell (Figure A.2) had to be purchased from Micrux Technologies (Oviedo, Spain).
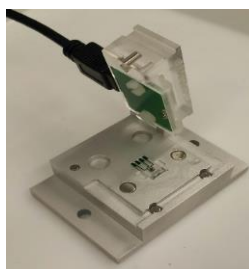
Figure A.2 - Cell used for application of micrux electrodes.

In order to use the evaporated electrodes, a cell had to be fabricated in-house in order to fix the glass slides, the gold electrodes could be exposed, as well as the pads (Figure A.3).

Figure A.3 - Cell used for the application of the evaporated electrodes.

B. EIS: nyquist plots and corresponding fittings

(a)

(b)

(c)

(d)

(e)

(f)

Figure B.1 - Nyquist plots of 1:29 ratio PNA/MCH immobilized gold working electrode, (a),(b) and (c) before and after incubation with 100 nM complementary ssDNA and (d), (e) and (f) without hybridization.

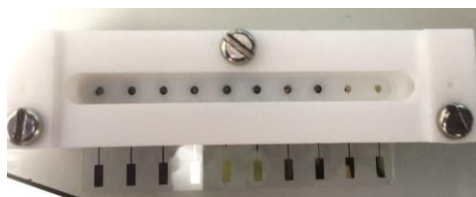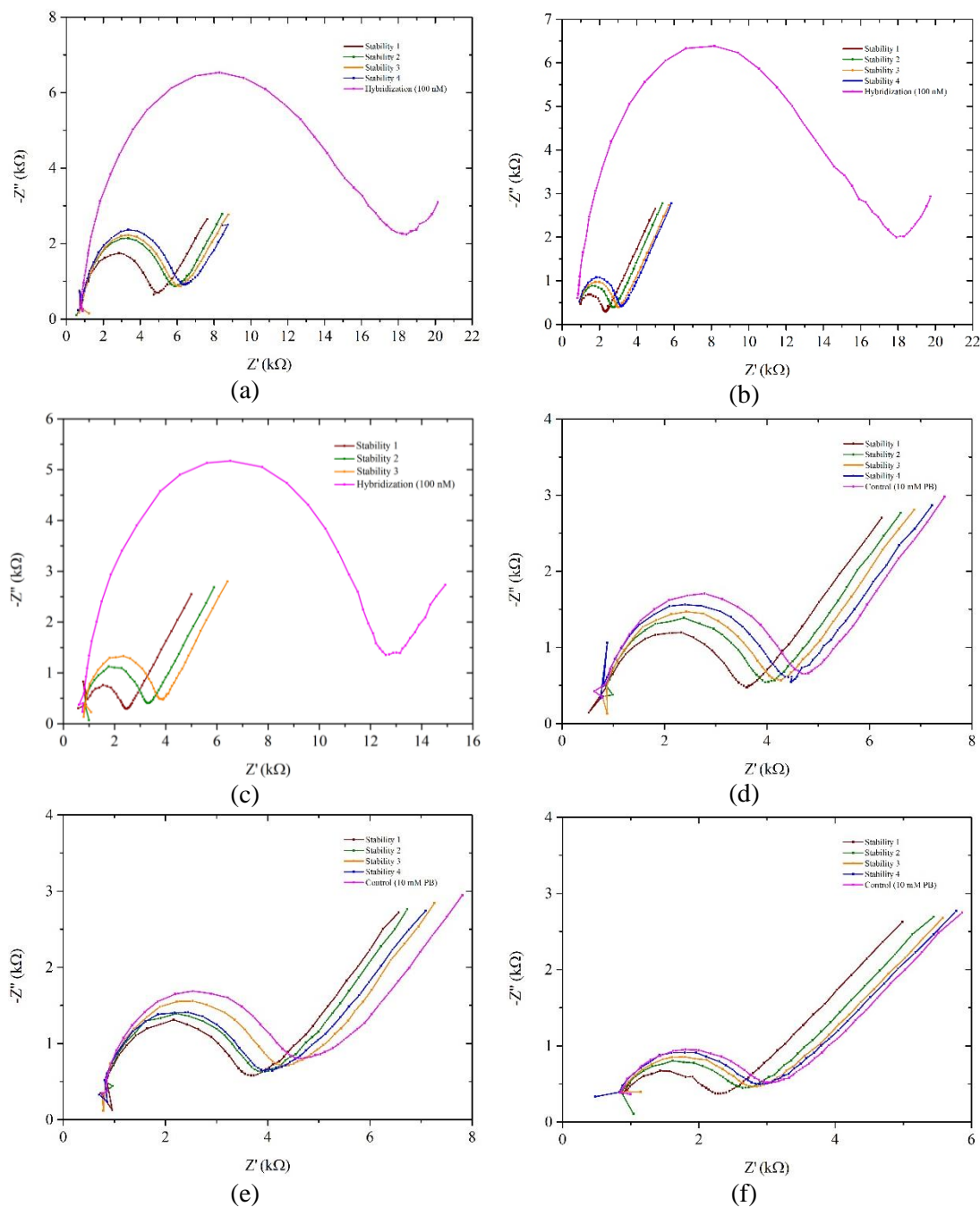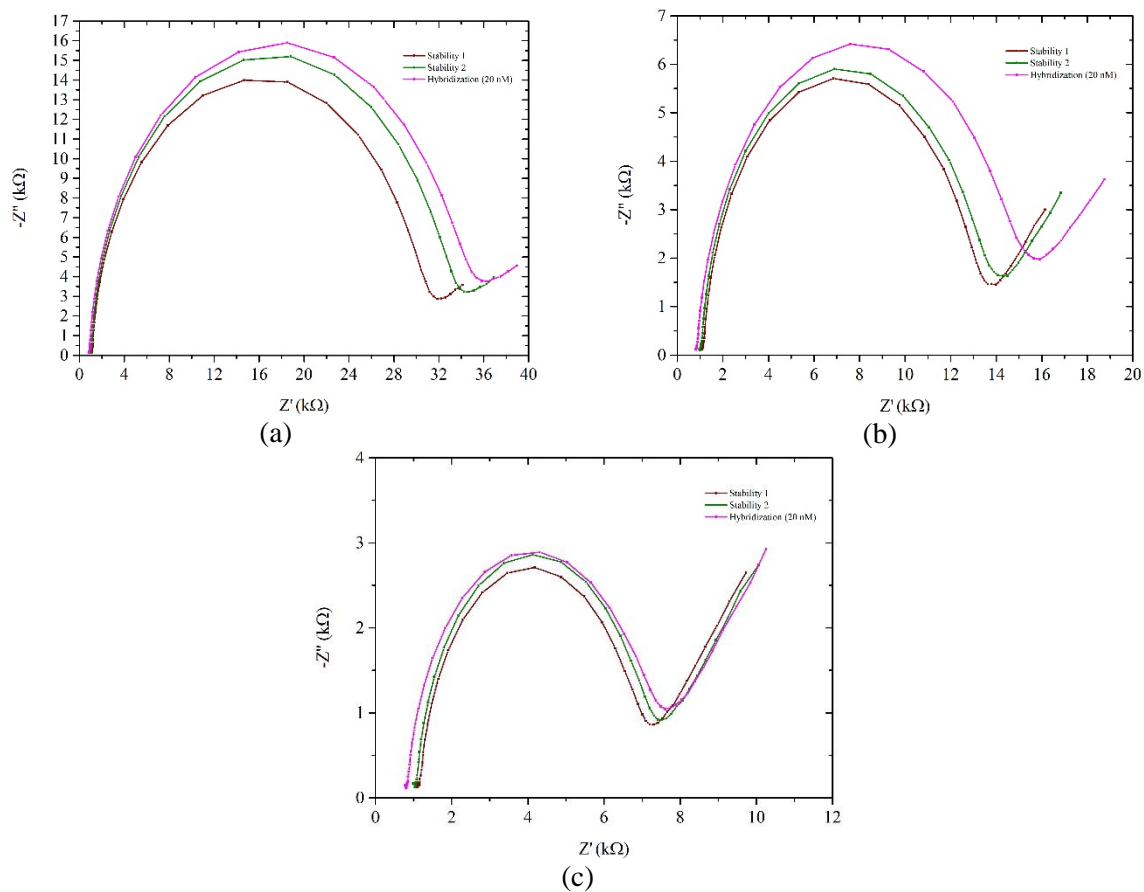| Parameters		R_s (kΩ)		R_{ct} (kΩ)		W (Ωs$^{-1/2}$)		Q (Ω^{-1}s^{-n})		n	
Electrode	Measurement	Value	Error (%)	Value	Error (%)	Value	Error (%)	Value	Error (%)	Value	Error (%)
(a)	Stability 1	675.0	5.8	4071.0	1.5	3.20×10^{-4}	1.94	8.17×10^{-7}	10.53	0.88	1.94
	Stability 2	708.1	4.43	4930.0	0.85	3.09×10^{-4}	0.96	7.66×10^{-7}	4.53	0.88	0.93
	Stability 3	710.7	4.83	5125.0	0.88	3.07×10^{-4}	0.98	7.70×10^{-7}	4.48	0.88	0.94
	Stability 4	648.0	6.52	5514.0	1.24	3.21×10^{-4}	2.23	7.97×10^{-7}	8.44	0.88	1.62
	Hybridization	542.7	14.54	16330	0.99	2.71×10^{-4}	4.36	9.58×10^{-7}	5.24	0.84	1.26
(b)	Stability 1	655.6	6.0	4101.0	1.36	3.21×10^{-4}	1.51	8.57×10^{-7}	8.38	0.87	1.63
	Stability 2	706.1	6.99	1935.0	3.08	3.07×10^{-4}	1.2	4.84×10^{-7}	18.88	0.90	3.15
	Stability 3	753.8	5.91	2157.0	2.45	3.11×10^{-4}	1.0	4.52×10^{-7}	13.71	0.92	2.35
	Stability 4	737.1	5.8	2320.0	2.27	3.12×10^{-4}	1.19	4.14×10^{-7}	14.49	0.92	2.38
	Hybridization	369.9	37.28	16320.0	1.42	2.79×10^{-4}	5.72	7.34×10^{-7}	7.42	0.82	1.77
(c)	Stability 1	536.6	11.33	1828.0	3.75	3.43×10^{-4}	1.0	5.90×10^{-7}	17.21	0.85	3.28
	Stability 2	706.8	4.11	2436.0	1.6	3.27×10^{-4}	1.22	4.06×10^{-7}	12.55	0.93	1.95
	Stability 3	732.6	4.57	2881.0	1.41	3.13×10^{-4}	0.89	3.85×10^{-7}	8.34	0.93	1.42
	Hybridization	640.3	5.64	11490.0	0.45	3.09×10^{-4}	1.45	4.06×10^{-7}	2.57	0.92	0.52
(d)	Stability 1	676.0	4.23	2755.0	1.24	3.19×10^{-4}	0.61	6.10×10^{-7}	6.14	0.89	1.18
	Stability 2	712.0	3.11	3188.0	0.9	3.17×10^{-4}	0.62	5.87×10^{-7}	5.21	0.90	0.95
	Stability 3	730.4	3.75	3273.0	1.0	3.08×10^{-4}	0.79	5.46×10^{-7}	6.27	0.91	1.13
	Stability 4	651.9	9.05	3579.0	2.41	3.03×10^{-4}	2.50	6.50×10^{-7}	17.6	0.88	3.09
	Control	659.4	3.2	3816.0	0.71	2.95×10^{-4}	0.6	5.50×10^{-7}	4.2	0.90	0.77
(e)	Stability 1	507.9	14.27	3188.0	2.72	3.08×10^{-4}	1.32	8.75×10^{-7}	12.24	0.82	2.64
	Stability 2	498.6	15.63	3413.0	2.76	3.04×10^{-4}	1.46	8.45×10^{-7}	12.62	0.82	2.71
	Stability 3	581.1	11.71	3739.0	2.34	2.97×10^{-4}	1.73	7.65×10^{-7}	12.84	0.84	2.55
	Stability 4	538.3	13.62	3508.0	2.67	3.01×10^{-4}	1.77	8.94×10^{-7}	14.15	0.82	2.9
	Control	629.8	7.8	4088.0	1.85	2.81×10^{-4}	2.0	8.61×10^{-7}	13.15	0.83	2.47
(f)	Stability 1	671.5	6.19	1623.0	3.74	3.25×10^{-4}	1.67	1.33×10^{-6}	27.77	0.82	4.89
	Stability 2	703.7	6.56	1958.0	2.98	3.16×10^{-4}	1.04	1.28×10^{-6}	15.42	0.82	3.1
	Stability 3	647.6	7.41	2168.0	2.8	3.21×10^{-4}	1.06	1.44×10^{-6}	14.04	0.80	2.96
	Stability 4	547.4	8.61	2366.0	2.42	3.11×10^{-4}	0.8	1.41×10^{-6}	10.36	0.79	2.35
	Control	673.2	4.79	2348.0	1.84	3.12×10^{-4}	0.92	1.25×10^{-6}	10.7	0.82	2.1

Table 1 - Fitting Values of the Equivalent Circuit Elements.

Figure B.2 - Nyquist plots of the impendence spectra obtained for the characterization of the PNA-DNA hybridization with a 1:29 ratio PNA/MCH evaporated gold electrodes with 20 nM DNA.

Parameters		R_s (kΩ)		R_{ct} (kΩ)		W (Ωs$^{-1/2}$)		Q (Ω^{-1}s^{-n})		n	
Electrode	Measurement	Value	Error (%)	Value	Error (%)	Value	Error (%)	Value	Error (%)	Value	Error (%)
(a)	Stability 1	1115.0	2.35	29300.0	0.19	2.58×10^{-4}	1.52	5.05×10^{-7}	0.91	0.97	0.21
	Stability 2	1026.0	2.97	31730.0	0.22	2.34×10^{-4}	1.81	5.02×10^{-7}	1.08	0.97	0.25
	Hybridization	871.7	9.29	33220.0	0.42	1.99×10^{-4}	2.4	5.21×10^{-7}	1.62	0.96	0.42
(b)	Stability 1	1152.0	1.48	11860.0	0.23	2.95×10^{-4}	0.8	5.26×10^{-7}	1.27	0.96	0.26
	Stability 2	1044.0	1.84	12330.0	0.26	2.62×10^{-4}	0.87	5.23×10^{-7}	1.5	0.96	0.31
	Hybridization	840.6	3.88	14000.0	0.41	2.42×10^{-4}	1.38	6.88×10^{-7}	2.17	0.93	0.48
(c)	Stability 1	1126.0	1.49	5765.0	0.5	3.29×10^{-4}	1.06	6.42×10^{-7}	3.51	0.94	0.64
	Stability 2	1045.0	1.49	6050.0	0.43	3.16×10^{-4}	0.92	6.26×10^{-7}	3.0	0.94	0.55
	Hybridization	799.4	1.69	6425.0	0.39	3.02×10^{-4}	0.86	8.32×10^{-7}	2.69	0.92	0.52

**Table 2 -** Fitting Values of the Equivalent Circuit Elements.

(a)

(b)

(c)

(d)
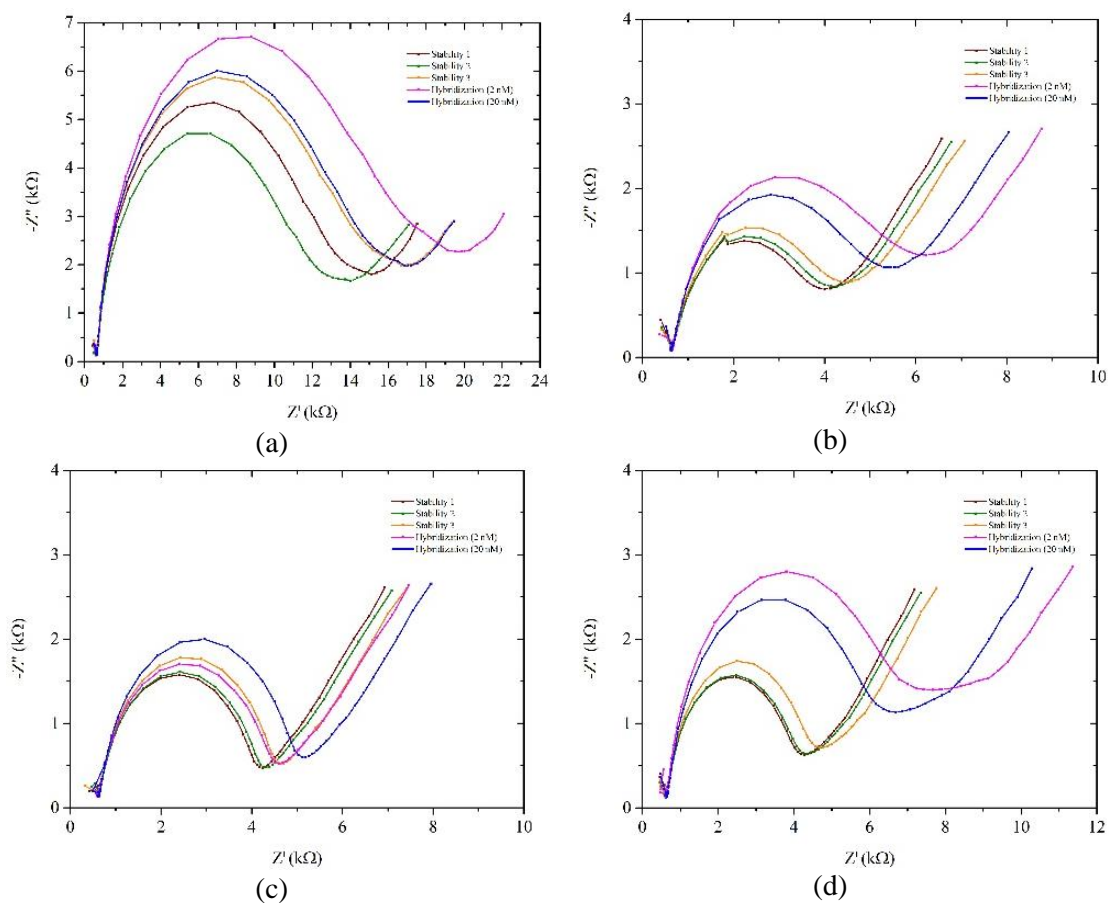
Figure B.3 – Nyquist ploys for gold working electrodes and a 1:29 ratio obtained before after incubation with 2 and 20 nM DNA.

Parameters		R_s (kΩ)		R_{ct} (kΩ)		W (Ωs$^{-1/2}$)		Q (Ω^{-1}s^{-n})		n	
Electrode	Measurement	Value	Error (%)	Value	Error (%)	Value	Error (%)	Value	Error (%)	Value	Error (%)
(a)	Stability 1	594.7	0.0	13280.0	1.13	2.61×10^{-4}	5.69	6.13×10^{-7}	9.84	0.84	1.9
	Stability 2	548.8	0.0	11230.0	0.0	2.01×10^{-4}	5.71	4.30×10^{-7}	16.43	0.89	2.96
	Stability 3	97.1	242.33	15500.0	2.31	2.60×10^{-4}	7.0	7.32×10^{-7}	11.14	0.80	2.77
	Hybridization (2 nM)	1.0×10^{-4}	1000	18260.0	2.95	2.49×10^{-4}	8.41	7.89×10^{-7}	11.75	0.78	3.28
	Hybridization (20 nM)	412.0	30.38	15240.0	1.51	2.53×10^{-4}	5.88	6.39×10^{-7}	9.34	0.82	2.05
(b)	Stability 1	589.0	4.67	3318.0	1.78	3.37×10^{-4}	2.09	2.23×10^{-6}	12.12	0.83	2.45
	Stability 2	603.8	4.12	3496.0	1.56	3.39×10^{-4}	1.92	2.39×10^{-6}	10.39	0.82	2.15
	Stability 3	561.1	9.23	3789.0	2.08	3.36×10^{-4}	1.82	2.35×10^{-6}	9.74	0.82	2.33
	Hybridization (2 nM)	592.1	4.7	5360.0	1.23	3.22×10^{-4}	2.2	2.28×10^{-6}	7.49	0.82	1.66
	Hybridization (20 nM)	599.0	4.5	4635.0	1.32	3.22×10^{-4}	2.08	2.07×10^{-6}	8.41	0.84	1.78
(c)	Stability 1	586.6	4.13	3520.0	1.07	3.26×10^{-4}	1.45	3.64×10^{-7}	10.05	0.90	1.55
	Stability 2	589.9	4.63	3621.0	1.18	3.27×10^{-4}	1.64	3.76×10^{-7}	11.01	0.90	1.71
	Stability 3	576.9	4.59	3950.0	1.06	3.23×10^{-4}	1.61	3.47×10^{-7}	9.79	0.91	1.52
	Hybridization (2 nM)	580.1	4.59	3941.0	1.08	3.19×10^{-4}	1.58	4.15×10^{-7}	9.84	0.89	1.57
	Hybridization (20 nM)	607.5	5.01	4413.0	1.11	3.16×10^{-4}	1.84	3.46×10^{-7}	10.07	0.91	1.59
(d)	Stability 1	607.9	2.6	3454.0	0.92	2.55×10^{-4}	2.84	4.57×10^{-7}	6.7	0.90	1.06
	Stability 2	628.6	0.0	3482.0	0.83	2.46×10^{-4}	3.7	4.42×10^{-7}	7.22	0.91	1.05
	Stability 3	628.1	0.0	371.3	0.0	2.75×10^{-4}	2.87	3.42×10^{-7}	21.14	0.95	3.09
	Hybridization (2 nM)	599.0	4.72	6295.0	1.23	1.46×10^{-4}	4.29	4.78×10^{-7}	7.47	0.90	1.27
	Hybridization (20 nM)	662.0	2.46	5351.0	0.75	1.51×10^{-4}	2.96	3.89×10^{-7}	3.96	0.93	0.65

Table 3 - Fitting Values of the Equivalent Circuit Elements.
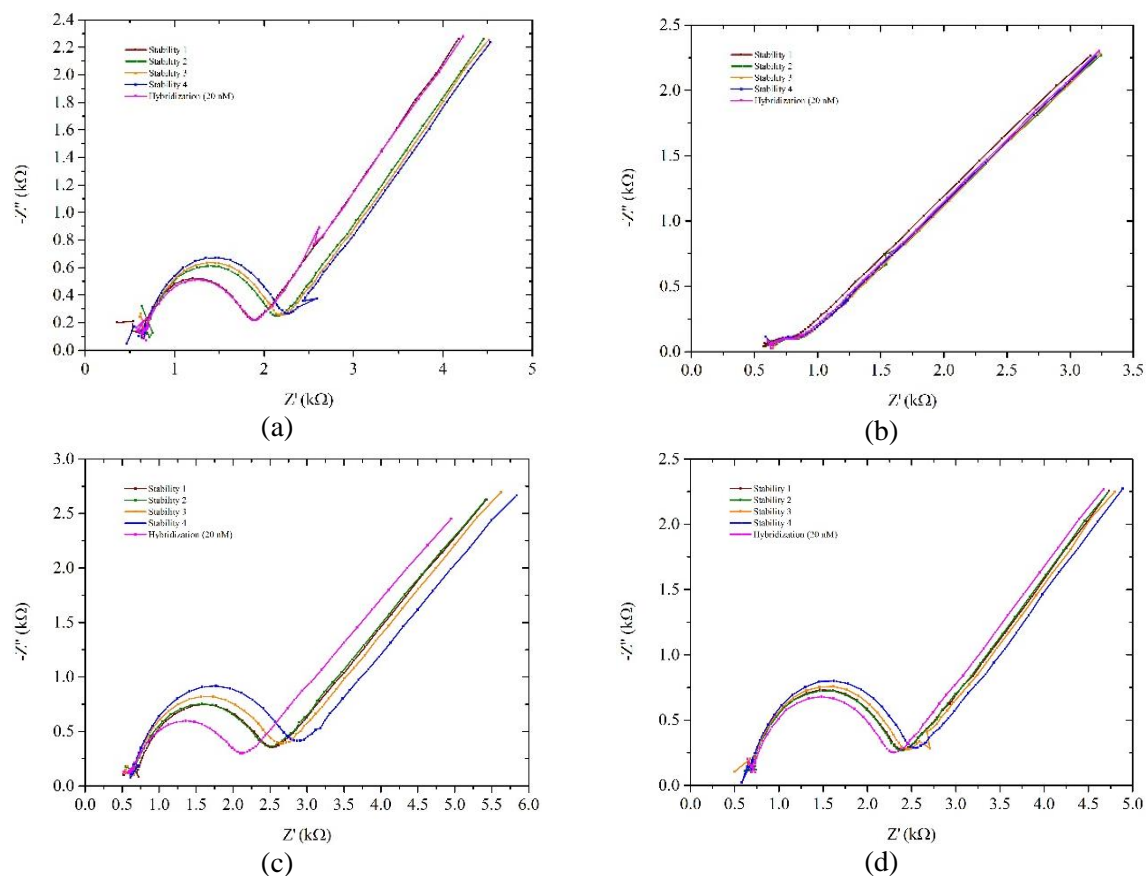
Figure B.4 – Nyquist plots for gold working electrodes, with a 1:29 ratio in which no PNA is in the immobilization solution, obtained before after incubation with 20 nM DNA.

Parameters		R_s (kΩ)		R_{ct} (kΩ)		W (Ωs$^{-1/2}$)		Q (Ω^{-1}s^{-n})		n	
Electrode	**Measurement**	**Value**	**Error (%)**	**Value**	**Error (%)**	**Value**	**Error (%)**	**Value**	**Error (%)**	**Value**	**Error (%)**
(a)	Stability 1	593.7	2.05	1237.0	1.3	3.85×10^{-4}	0.55	6.75×10^{-7}	11.03	0.85	1.69
	Stability 2	647.2	2.22	1442.0	1.39	3.82×10^{-4}	0.75	6.64×10^{-7}	12.45	0.86	1.9
	Stability 3	621.9	1.92	1507.0	1.08	3.82×10^{-4}	0.58	6.51×10^{-7}	9.14	0.86	1.42
	Stability 4	621.1	2.36	1572.0	1.25	3.87×10^{-4}	0.7	6.02×10^{-7}	10.4	0.87	1.61
	Hybridization (20 nM)	612.2	3.2	1229.0	2.05	3.81×10^{-4}	0.77	7.06×10^{-7}	16.08	0.85	2.52
(b)	Stability 1	551.9	2.76	276.9	14.6	3.77×10^{-4}	2.09	9.97×10^{-6}	92.62	0.70	15.9
	Stability 2	620.6	2.6	282.1	11.93	3.78×10^{-4}	1.5	9.67×10^{-6}	68.5	0.70	12.48
	Stability 3	616.0	2.01	295.5	9.35	3.78×10^{-4}	1.25	1.05×10^{-5}	52.55	0.70	9.66
	Stability 4	586.9	11.97	311.2	51.88	3.81×10^{-4}	6.71	8.41×10^{-6}	354.19	0.70	61.24
	Hybridization (20 nM)	603.2	2.12	277.9	10.9	3.73×10^{-4}	2.08	1.08×10^{-5}	61.39	0.70	11.09
(c)	Stability 1	638.6	5.16	1876.0	2.29	3.17×10^{-4}	0.95	1.01×10^{-6}	14.87	0.81	2.7
	Stability 2	597.7	3.71	1893.0	1.88	3.16×10^{-4}	1.16	1.09×10^{-6}	16.64	0.81	2.79
	Stability 3	591.5	4.37	2025.0	1.79	3.07×10^{-4}	0.93	9.42×10^{-7}	13.16	0.83	2.29
	Stability 4	613.5	5.61	2210.0	2.53	3.09×10^{-4}	1.89	8.66×10^{-7}	22.53	0.84	3.71
	Hybridization (20 nM)	550.3	7.45	1592.0	3.4	3.37×10^{-4}	1.84	1.43×10^{-6}	21.56	0.77	4.06
(d)	Stability 1	644.3	2.73	1698.0	1.31	3.8×10^{-4}	0.68	5.29×10^{-7}	9.87	0.87	1.56
	Stability 2	674.4	3.52	1626.0	1.86	3.78×10^{-4}	1.68	2.94×10^{-7}	5.51	0.91	0.0
	Stability 3	649.0	2.47	1747.0	1.19	3.8×10^{-4}	0.68	5.04×10^{-7}	9.36	0.95	1.46
	Stability 4	641.5	2.35	1833.0	1.07	3.79×10^{-4}	0.65	4.88×10^{-7}	8.46	0.88	1.32
	Hybridization (20 nM)	671.3	2.05	1568.0	0.75	3.78×10^{-4}	0.66	5.25×10^{-7}	10.15	0.87	1.54

Table 4 - Fitting Values of the Equivalent Circuit Elements.